



# Lawrence Berkeley Laboratory

UNIVERSITY OF CALIFORNIA

## Materials & Molecular Research Division

Submitted to Physical Review

TRANSIENT FOUR-WAVE MIXING AND COHERENT  
TRANSIENT OPTICAL PHENOMENA

Peixian Ye and Y.R. Shen

September 1981

RECEIVED  
LAWRENCE  
BERKELEY LABORATORY

NOV 13 1981

LIBRARY AND  
DOCUMENTS SECTION

### TWO-WEEK LOAN COPY

*This is a Library Circulating Copy  
which may be borrowed for two weeks.  
For a personal retention copy, call  
Tech. Info. Division, Ext. 6782*



LBL-13462  
c.2

## **DISCLAIMER**

This document was prepared as an account of work sponsored by the United States Government. While this document is believed to contain correct information, neither the United States Government nor any agency thereof, nor the Regents of the University of California, nor any of their employees, makes any warranty, express or implied, or assumes any legal responsibility for the accuracy, completeness, or usefulness of any information, apparatus, product, or process disclosed, or represents that its use would not infringe privately owned rights. Reference herein to any specific commercial product, process, or service by its trade name, trademark, manufacturer, or otherwise, does not necessarily constitute or imply its endorsement, recommendation, or favoring by the United States Government or any agency thereof, or the Regents of the University of California. The views and opinions of authors expressed herein do not necessarily state or reflect those of the United States Government or any agency thereof or the Regents of the University of California.

TRANSIENT FOUR-WAVE MIXING AND COHERENT TRANSIENT  
OPTICAL PHENOMENA\*

Peixian Ye

Institute of Physics, Academy of Sciences  
Beijing, China

and

Y. R. Shen<sup>†</sup>

Department of Physics, University of California  
Berkeley, California 94720

and

Materials and Molecular Research Division  
Lawrence Berkeley Laboratory, Berkeley, California 94720

SEPTEMBER 1981

ABSTRACT

The general formalism of transient four-wave mixing is developed using the diagrammatic technique of Yee and Gustafson, and applied systematically to two-, three-, and four-level systems. The results predict all possible photon echo phenomena including free induction decay in the low-intensity limit. Connections to transient saturation spectroscopy and other coherent transient effects can also be made. The treatment can be readily extended to the more general problem of coherent transient optical effects with  $n$  waves.

---

\* This work was supported by the Director, Office of Energy Research, Office of Basic Energy Sciences, Materials Sciences Division of the U.S. Department of Energy under Contract No. W-7405-ENG-48.

<sup>†</sup> Acknowledges a research professorship from the Miller Institute of the University of California.

## I. Introduction

Four-wave mixing has recently become one of the most interesting and thoroughly investigated nonlinear optical effects.<sup>1</sup> It is a process that is allowed in all media, and has therefore found numerous important applications. Because of the inherent resonant enhancement feature, it has attracted a great deal of attention as a new modern spectroscopic technique. Druet et al.<sup>2</sup> have studied resonant four-wave mixing in some cases. Oudar and Shen<sup>3</sup> have given a more general analysis of the various multi-resonant four-wave mixing processes. It is shown that with appropriate arrangement, four-wave mixing can be used to obtain Doppler-free spectra or spectra with reduced inhomogeneous broadening, to study transitions between excited states, to measure longitudinal and transverse relaxation times, etc. The analysis is, however, restricted to the steady-state case. We then realize that with time as an additional variable, transient four-wave mixing can be much more interesting. In this paper, we give a general formulation of transient four-wave mixing. We derive and discuss the results of many such processes in two-, three-, and four-level systems, and show their connection with the known photon echo phenomena.<sup>4,5</sup>

In general, transient four-wave mixing deals with the situation where three input pulsed fields of either the same or different frequencies excite a medium successively in a given time order. The radiative output, which is the fourth wave, shows a time variation depending on the time sequence and separation of the input pulses. In special cases, the input pulses can coincide in time and can be of the same frequency. The transient behavior arises because the medium is resonantly or near-reson-

antly excited by the input pulses. It is, therefore, dominated by the dephasing (transverse) relaxation of coherent excitation between relevant levels, and sometimes also by the population (longitudinal) relaxation. Experiments on transient four-wave mixing can be used not only to study the particular time-ordered four-wave mixing process itself, but also to obtain the various relaxation rates in the medium.

Transient four-wave mixing can be considered as a special class of coherent transient optical effects. That coherent transient optical effects can be used to study relaxation phenomena in a medium is, of course, well known. As we shall see later, transient four-wave mixing actually covers the various known cases of photon echoes,<sup>4</sup> including tri-level echo, stimulated echo, backward echo, etc., although usually the echo phenomena are discussed in terms of the vector model of excitation in a non-perturbative approach. This is easily demonstrated in the perturbation limit when four-wave mixing can be treated as a third-order process with no pump saturation. (In this paper, we shall consider only four-wave mixing with no pump saturation.)

On the other hand, transient four-wave mixing is more general and predicts coherent transient effects other than the photon echo phenomena. It covers, for example, cases such as free-induction decay, transient coherent Raman scattering, transient optical-field induced effect, etc. In order to make a thorough investigation of all possible cases of transient four-wave mixing, a systematic study starting from a general formulation is needed.

In Sec. II, the general formulation of transient four-wave mixing is given. We briefly review the diagrammatic technique of Yee and Gustafson

used to derive the time-dependent third-order nonlinear polarization responsible for a transient four-wave mixing process.<sup>6</sup> We then discuss how the Doppler broadening or inhomogeneous broadening causes dephasing and rephasing of a coherent excitation, and how the result yields the conditions for the appearance of a pulsed four-wave mixing output. In Sec. III, the general formulation is used to analyze the various cases of transient four-wave mixing in two-, three-, and four-level systems. Only triply resonant cases will be discussed in this paper. The results are tabulated, and those cases which correspond to known transient effects are identified. Finally, In Sec. IV, how the various transient four-wave mixing processes can be used to measure material properties contributing to the relaxation of material excitation is discussed.

## II. General Formulation

In the limit of no pumping saturation, the four-wave mixing output is governed by the third-order nonlinear polarization  $\vec{P}^{(3)}(\omega)$ , which is related to the third-order density matrix  $\rho^{(3)}(\omega)$  by

$$\vec{P}^{(3)}(\omega) = \text{Tr}[-e\vec{r}\rho^{(3)}(\omega)]. \quad (1)$$

Thus, the main step in the theory of four-wave mixing is to find  $\rho^{(3)}(\omega)$ . In the transient cases,  $\rho^{(3)}(\omega)$  is also a function of time.

### A. Diagrammatic Technique

We adopt here the diagrammatic technique of Yee and Gustafson<sup>6</sup> to find  $\rho^{(3)}$ . The notations follow those of Ref. 6. We consider the general case where three successive pulses with field amplitudes  $\vec{E}_1(\omega_1)$ ,  $\vec{E}_2(\omega_2)$ ,

$\vec{\mathcal{E}}_3(\omega_3)$  interact with the material system at  $t_1, t_2, t_3$  with  $t_1 < t_2 < t_3$ . In this given time order,  $\rho^{(3)}(\omega)$  has 8 terms derived from the 8 diagrams in Fig. 1. The rules for deriving an expression from a diagram are as follows. (1) A vertex on the left of the circle with the material system changing from  $\langle n|$  to  $\langle n'|$  at time  $t$  contributes to the expression a matrix element  $\langle n'|H'(t)/i\hbar|n\rangle$ . We have  $H'(t) = -\frac{1}{2}\vec{\mu} \cdot \vec{\mathcal{E}}(\omega)e^{-i\omega t}$  for absorption and  $H'(t) = -\frac{1}{2}\vec{\mu} \cdot \vec{\mathcal{E}}^*(\omega)e^{+i\omega t}$  for emission. If the vertex appears on the right of the circle, then  $\langle n|H'(t)/i\hbar|n'\rangle^*$  should be used instead. (2) Propagation from one vertex at  $t_i$  to the next at  $t_j$  contributes a factor  $\langle ab|\hat{A}(t_j - t_i)|ab\rangle = e^{-i(\omega_{ab} + \phi_{ab}^i)(t_j - t_i)}$ , where  $|a\rangle$  is the ket state on the left of the circle and  $\langle b|$  is the bra state on the right, and

$$\phi_{ab} = \phi_{ba}^* = \gamma_{ab} + i\Delta_{ab} \quad (2)$$

arises from damping of the material excitation. We assume that even the population excitation in a given state decays exponentially with time.

(3) The product of all factors is integrated over all possible time separations between vertices and summed over all possible initial, intermediate, and final states. In Fig. 1, the material system is assumed to start from  $|m\rangle\langle m|$  and end up at  $|p\rangle\langle s|$ ,  $|p\rangle\langle m|$ , or  $|m\rangle\langle s|$ . The initial time  $t_0$  is set at  $-\infty$ .

Following the above rules, we can find, for example, from Fig. 1a,

$$[\rho^{(3)}(t)]_{(a)} = \sum_{m,r,p,s} \left\{ \int_{-\infty}^0 d\tau_1 \int_{-\infty}^0 d\tau_2 \int_{-\infty}^0 d\tau_3 \right.$$

cont'd

$$\begin{aligned}
& \times e^{-(i\omega_{ps} + \phi_{ps})\tau_3} e^{-(i\omega_{pr} + \phi_{pr})\tau_2} e^{-(i\omega_{pm} + \phi_{pm})\tau_1} \\
& \times \langle p | \frac{-1}{2i\hbar} \vec{\mu} \cdot \vec{\hat{e}}_1 (t - \tau_1 - \tau_2 - \tau_3) e^{-i\omega_1(t - \tau_1 - \tau_2 - \tau_3)} | m \rangle \\
& \times \langle m | \frac{-1}{-2i\hbar} \vec{\mu} \cdot \vec{\hat{e}}_2 (t - \tau_2 - \tau_3) e^{-i\omega_2(t - \tau_2 - \tau_3)} | r \rangle \\
& \times \langle r | \frac{-1}{-2i\hbar} \vec{\mu} \cdot \vec{\hat{e}}_3 (t - \tau_3) e^{-i\omega_3(t - \tau_3)} | s \rangle \left( | p \rangle \rho_{mm}^0 \langle s | \right) \Big\} . \quad (3)
\end{aligned}$$

With the substitution of variables  $\xi_1 \equiv t - \tau_1 - \tau_2 - \tau_3$ ,  $\xi_2 \equiv t - \tau_2 - \tau_3$ , and  $\xi_3 \equiv t - \tau_3$ , the above equation can be rewritten as

$$\begin{aligned}
[\rho^{(3)}(t)]_{(a)} &= - \sum_{m,r,p,s} \left\{ e^{-(i\omega_{ps} + \phi_{ps})t} \left( \frac{1}{2i\hbar} \right)^3 \left( | p \rangle \rho_{mm}^0 \langle s | \right) \right. \\
& \times \langle p | \vec{\mu} \cdot \hat{e}_1 | m \rangle \langle m | \vec{\mu} \cdot \hat{e}_2 | r \rangle \langle r | \vec{\mu} \cdot \hat{e}_3 | s \rangle \\
& \times \int_{-\infty}^t d\xi_3 e^{[(i\omega_{ps} + \phi_{ps}) - (i\omega_{pr} + \phi_{pr}) - i\omega_3]\xi_3} \hat{e}_3(\xi_3) \\
& \times \int_{-\infty}^{\xi_3} d\xi_2 e^{[(i\omega_{pr} + \phi_{pr}) - (i\omega_{pm} + \phi_{pm}) - i\omega_2]\xi_2} \hat{e}_2(\xi_2) \\
& \times \left. \int_{-\infty}^{\xi_2} d\xi_1 e^{[(i\omega_{pm} + \phi_{pm}) - i\omega_1]\xi_1} \hat{e}_1(\xi_1) \right\} . \quad (4a)
\end{aligned}$$

Similarly, we find from Fig. 1b-h respectively,

$$[\rho^{(3)}(t)]_{(b)} = \sum_{m,r,p,s} \left\{ e^{-(i\omega_{ps} + \phi_{ps})t} \left( \frac{1}{2i\hbar} \right)^3 \left( | p \rangle \rho_{mm}^0 \langle s | \right) \right.$$

cont'd

$$\begin{aligned}
& \times \langle p | \vec{\mu} \cdot \hat{e}_2 | r \rangle \langle r | \vec{\mu} \cdot \hat{e}_1 | m \rangle \langle m | \vec{\mu} \cdot \hat{e}_3 | s \rangle \\
& \times \int_{-\infty}^t d\xi_3 e^{[(i\omega_{ps} + \phi_{ps}) - (i\omega_{pm} + \phi_{pm}) - i\omega_3] \xi_3} \xi_3 \mathcal{E}_3(\xi_3) \\
& \times \int_{-\infty}^{\xi_3} d\xi_2 e^{[(i\omega_{pm} + \phi_{pm}) - (i\omega_{rm} + \phi_{rm}) - i\omega_2] \xi_2} \xi_2 \mathcal{E}_2(\xi_2) \\
& \times \int_{-\infty}^{\xi_2} d\xi_1 e^{[(i\omega_{rm} + \phi_{rm}) - i\omega_1] \xi_1} \xi_1 \mathcal{E}_1(\xi_1) \Big\} \tag{4b}
\end{aligned}$$

$$\begin{aligned}
[\rho^{(3)}(t)]_{(c)} &= \sum_{m,r,p,s} \left\{ e^{-(i\omega_{ps} + \phi_{ps})t} \left( \frac{1}{2i\hbar} \right)^3 (|p\rangle \rho_{mm}^0 \langle s|) \right. \\
& \times \langle p | \vec{\mu} \cdot \hat{e}_3 | r \rangle \langle r | \vec{\mu} \cdot \hat{e}_1 | m \rangle \langle m | \vec{\mu} \cdot \hat{e}_2 | s \rangle \\
& \times \int_{-\infty}^t d\xi_3 e^{[(i\omega_{ps} + \phi_{ps}) - (i\omega_{rs} + \phi_{rs}) - i\omega_3] \xi_3} \xi_3 \mathcal{E}_3(\xi_3) \\
& \times \int_{-\infty}^{\xi_3} d\xi_2 e^{[(i\omega_{rs} + \phi_{rs}) - (i\omega_{rm} + \phi_{rm}) - i\omega_2] \xi_2} \xi_2 \mathcal{E}_2(\xi_2) \\
& \times \int_{-\infty}^{\xi_2} d\xi_1 e^{[(i\omega_{rm} + \phi_{rm}) - i\omega_1] \xi_1} \xi_1 \mathcal{E}_1(\xi_1) \Big\} \tag{4c}
\end{aligned}$$

$$\begin{aligned}
[\rho^{(3)}(t)]_{(d)} &= - \sum_{m,r,p,s} \left\{ e^{-(i\omega_{pm} + \phi_{pm})t} \left( \frac{1}{2i\hbar} \right)^3 (|p\rangle \rho_{mm}^0 \langle m|) \right. \\
& \times \langle p | \vec{\mu} \cdot \hat{e}_3 | r \rangle \langle r | \vec{\mu} \cdot \hat{e}_2 | n \rangle \langle n | \vec{\mu} \cdot \hat{e}_1 | m \rangle \\
& \times \int_{-\infty}^t d\xi_3 e^{[(i\omega_{pm} + \phi_{pm}) - (i\omega_{rm} + \phi_{rm}) - i\omega_3] \xi_3} \xi_3 \mathcal{E}_3(\xi_3) \\
& \times \int_{-\infty}^{\xi_3} d\xi_2 e^{[(i\omega_{rm} + \phi_{rm}) - (i\omega_{nm} + \phi_{nm}) - i\omega_2] \xi_2} \xi_2 \mathcal{E}_2(\xi_2)
\end{aligned}$$

cont'd

$$\times \int_{-\infty}^{\xi_2} d\xi_1 e^{[(i\omega_{nm} + \phi_{nm}) - i\omega_1] \xi_1} \xi_1 \xi_1(\xi_1) \Big\} \quad (4d)$$

$$[\rho^{(3)}(t)]_{(e)} = \sum_{m,r,p,s} \left\{ e^{-(i\omega_{ps} + \phi_{ps})t} \left( \frac{1}{2i\hbar} \right)^3 (|p\rangle \rho_{mm}^0 \langle s|) \right. \\ \times \langle p | \vec{\mu} \cdot \hat{e}_3 | r \rangle \langle r | \vec{\mu} \cdot \hat{e}_2 | m \rangle \langle m | \vec{\mu} \cdot \hat{e}_1 | s \rangle \\ \times \int_{-\infty}^t d\xi_3 e^{[(i\omega_{ps} + \phi_{ps}) - (i\omega_{rs} + \phi_{rs}) - i\omega_3] \xi_3} \xi_3 \xi_3(\xi_3) \\ \times \int_{-\infty}^{\xi_3} d\xi_2 e^{[(i\omega_{rs} + \phi_{rs}) - (i\omega_{ms} + \phi_{ms}) - i\omega_2] \xi_2} \xi_2 \xi_2(\xi_2) \\ \times \int_{-\infty}^{\xi_2} d\xi_1 e^{[(i\omega_{ms} + \phi_{ms}) - i\omega_1] \xi_1} \xi_1 \xi_1(\xi_1) \Big\} \quad (4e)$$

$$[\rho^{(3)}(t)]_{(f)} = - \sum_{m,r,p,s} \left\{ e^{-(i\omega_{ps} + \phi_{ps})t} \left( \frac{1}{2i\hbar} \right)^3 (|p\rangle \rho_{mm}^0 \langle s|) \right. \\ \times \langle p | \vec{\mu} \cdot \hat{e}_3 | m \rangle \langle m | \vec{\mu} \cdot \hat{e}_1 | r \rangle \langle r | \vec{\mu} \cdot \hat{e}_2 | s \rangle \\ \times \int_{-\infty}^t d\xi_3 e^{[(i\omega_{ps} + \phi_{ps}) - (i\omega_{ms} + \phi_{ms}) - i\omega_3] \xi_3} \xi_3 \xi_3(\xi_3) \\ \times \int_{-\infty}^{\xi_3} d\xi_2 e^{[(i\omega_{ms} + \phi_{ms}) - (i\omega_{mr} + \phi_{mr}) - i\omega_2] \xi_2} \xi_2 \xi_2(\xi_2) \\ \times \int_{-\infty}^{\xi_2} d\xi_1 e^{[(i\omega_{mr} + \phi_{mr}) - i\omega_1] \xi_1} \xi_1 \xi_1(\xi_1) \Big\} \quad (4f)$$

$$[\rho^{(3)}(t)]_{(g)} = - \sum_{m,r,p,s} \left\{ e^{-(i\omega_{ps} + \phi_{ps})t} \left( \frac{1}{2i\hbar} \right)^3 (|p\rangle \rho_{mm}^0 \langle s|) \right. \\ \times \langle p | \vec{\mu} \cdot \hat{e}_2 | m \rangle \langle m | \vec{\mu} \cdot \hat{e}_1 | r \rangle \langle r | \vec{\mu} \cdot \hat{e}_3 | s \rangle$$

$$\begin{aligned}
& \times \int_{-\infty}^t d\xi_3 e^{[(i\omega_{ps} + \phi_{ps}) - (i\omega_{pr} + \phi_{pr}) - i\omega_3]\xi_3} \xi_3 \xi_3(\xi_3) \\
& \times \int_{-\infty}^{\xi_3} d\xi_2 e^{[(i\omega_{pr} + \phi_{pr}) - (i\omega_{mr} + \phi_{mr}) - i\omega_2]\xi_2} \xi_2 \xi_2(\xi_2) \\
& \times \int_{-\infty}^{\xi_2} d\xi_1 e^{[(i\omega_{mr} + \phi_{mr}) - i\omega_1]\xi_1} \xi_1 \xi_1(\xi_1) \Big\} \quad (4g)
\end{aligned}$$

$$\begin{aligned}
[\rho^{(3)}(t)]_{(h)} &= \sum_{m,r,p,s} \left\{ e^{-(i\omega_{ms} + \phi_{ms})t} \left( \frac{1}{2i\hbar} \right)^3 (|m\rangle \rho_{mm}^0 \langle s|) \right. \\
& \times \langle m | \vec{\mu} \cdot \hat{e}_1 | n \rangle \langle n | \vec{\mu} \cdot \hat{e}_2 | r \rangle \langle r | \vec{\mu} \cdot \hat{e}_3 | s \rangle \\
& \times \int_{-\infty}^t d\xi_3 e^{[(i\omega_{ms} + \phi_{ms}) - (i\omega_{mr} + \phi_{mr}) - i\omega_3]\xi_3} \xi_3 \xi_3(\xi_3) \\
& \times \int_{-\infty}^{\xi_3} d\xi_2 e^{[(i\omega_{mr} + \phi_{mr}) - (i\omega_{mn} + \phi_{mn}) - i\omega_2]\xi_2} \xi_2 \xi_2(\xi_2) \\
& \times \int_{-\infty}^{\xi_2} d\xi_1 e^{[(i\omega_{mn} + \phi_{mn}) - i\omega_1]\xi_1} \xi_1 \xi_1(\xi_1) \Big\} \quad (4h)
\end{aligned}$$

The full expression of  $\rho^{(3)}(\omega = \omega_1 + \omega_2 + \omega_3, t)$  is then the sum of Eqs. (4a)-(4h). In an actual transient four-wave mixing case, resonant or near resonant excitations are involved. Therefore, the nonresonant terms in  $\rho^{(3)}(t)$  can be neglected, and the effective number of terms in  $\rho^{(3)}(t)$  is greatly reduced, as we shall see in Sec. III.

#### B. Doppler Effect

In a gaseous system,  $\rho^{(3)}(t)$  is different for molecules in different velocity groups. The difference arises from the fields seen by molecules with different velocities. At time  $t$ , let a molecule with velocity  $\vec{v}$  be

at the position  $\vec{r}(t)$ . Then at an earlier time  $\xi_1$ , the molecule is at  $\vec{r}(\xi_1) = \vec{r}(t) - \vec{v}(t - \xi_1)$ . Assume that the input pulses are plane waves. The field  $\mathcal{E}_i$  seen by the molecule at  $\vec{r}(\xi_1)$  is

$$\begin{aligned}\mathcal{E}_i(\xi_1) &= A_i(\xi_1) \exp[i\vec{k}_i \cdot \vec{r}(\xi_1)] \\ &= A_i(\xi_1) \exp[i\vec{k}_i \cdot \vec{r}(t) - i(\vec{k}_i \cdot \vec{v})(t - \xi_1)].\end{aligned}\quad (5)$$

With this expression of  $\mathcal{E}_i(\xi_1)$  in Eq. (5),  $\rho^{(3)}(t)$  for the molecule becomes also a function of  $\vec{v}$ . For example, we have from Eq. (4a)

$$\begin{aligned}[\rho^{(3)}(\vec{v}; t)]_{(a)} &= - \sum_{m, r, p, s} \left\{ e^{-(i\omega_{ps} + \phi_{ps})t} \left(\frac{1}{2i\hbar}\right)^3 |p\rangle_{mm}^o \langle s| \right. \\ &\quad \times \langle p | \vec{\mu} \cdot \hat{e}_1 | m \rangle \langle m | \vec{\mu} \cdot \hat{e}_2 | r \rangle \langle r | \vec{\mu} \cdot \hat{e}_3 | s \rangle \\ &\quad \times e^{i(\vec{k}_1 + \vec{k}_2 + \vec{k}_3) \cdot [\vec{r}(t) - \vec{v}t]} \\ &\quad \times \int_{-\infty}^t d\xi_3 e^{[i(\omega_{rs} - \omega_3) + \phi_{ps} - \phi_{pr} + i\vec{k}_3 \cdot \vec{v}] \xi_3} A_3(\xi_3) \\ &\quad \times \int_{-\infty}^{\xi_3} d\xi_2 e^{[i(\omega_{mr} - \omega_2) + \phi_{pr} - \phi_{pm} + i\vec{k}_2 \cdot \vec{v}] \xi_2} A_2(\xi_2) \\ &\quad \times \left. \int_{-\infty}^{\xi_2} d\xi_1 e^{[i(\omega_{pm} - \omega_1) + \phi_{pm} + i\vec{k}_1 \cdot \vec{v}] \xi_1} A_1(\xi_1) \right\}.\end{aligned}\quad (6)$$

In actual evaluation of the integrals in Eq. (6), two special cases are of interest. In the first case, all successive pulse excitations are at resonance or near resonance, and the pulses are short enough so

that we can write

$$\begin{aligned} & \int_{-\infty}^{\xi} d\xi' e^{[i(\omega_{ij} - \omega_n) + \phi_{ij} + i\vec{k}_n \cdot \vec{v}]\xi'} A(\xi') \\ & \cong e^{(\phi_{ij} + i\vec{k}_n \cdot \vec{v})\xi_0} \int_{-\infty}^{\xi} d\xi' e^{i(\omega_{ij} - \omega_n)\xi'} A(\xi') \end{aligned} \quad (7)$$

where  $\xi_0$  indicates the time when the center of the pulse arrives at  $\vec{r}(t)$ .

Equation (6) then reduces to

$$\begin{aligned} [\rho^{(3)}(\vec{v}, t)]_{(a)} &= - \left( \frac{1}{2i\hbar} \right)^3 |p\rangle\langle s| e^{-i\omega_{ps}t + i(\vec{k}_1 + \vec{k}_2 + \vec{k}_3) \cdot \vec{r}} \\ & \times e^{-i\vec{v} \cdot [\vec{k}_3(t - \xi_{30}) + \vec{k}_2(t - \xi_{20}) + \vec{k}_1(t - \xi_{10})]} \\ & \times \sum_{m, r, p, s} \left\{ e^{-\phi_{ps}(t - \xi_{30}) - \phi_{pr}(\xi_{30} - \xi_{20}) - \phi_{pm}(\xi_{20} - \xi_{10})} \right. \\ & \times \langle p | \vec{\mu} \cdot \hat{e}_1 | m \rangle \langle m | \vec{\mu} \cdot \hat{e}_2 | r \rangle \langle r | \vec{\mu} \cdot \hat{e}_3 | s \rangle \\ & \times \int_{-\infty}^t d\xi_3 e^{i(\omega_{rs} - \omega_3)\xi_3} A_3(\xi_3) \\ & \times \int_{-\infty}^{\xi_3} d\xi_2 e^{i(\omega_{mr} - \omega_2)\xi_2} A_2(\xi_2) \\ & \left. \times \int_{-\infty}^{\xi_2} d\xi_1 e^{i(\omega_{pm} - \omega_1)\xi_1} A_1(\xi_1) \rho_{mm}^0 \right\}. \end{aligned} \quad (8)$$

In the second case, a particular pulse in the sequence of pulses may be far from inducing a resonant excitation. The corresponding integral in the form of  $\int_{-\infty}^{\xi} d\xi' \exp\{[i(\omega_{ij} - \omega_n) + \phi_{ij} + i\vec{k}_n \cdot \vec{v}]\xi'\} f(\xi')$  can be ap-

proximated by<sup>6</sup>  $f(\xi)/i[(\omega_{ij} - \omega_n + \vec{k}_n \cdot \vec{v}) - i\phi_{ij}]$ . The more general case would often require a more exact evaluation of the integrals in Eq. (6). In this paper, unless specified otherwise, we shall only consider the case where all pulses are at resonance such that Eq. (7) is valid.

Since  $\rho^{(3)}(\vec{v}, t)$  represents the radiating dipole induced by the input pulses on the molecule with velocity  $\vec{v}$ , its phase factor describes the phase of the dipole radiation field. As seen in Eq. (8), the only phase factor in  $\rho^{(3)}(\vec{v}, t)$  depending on  $\vec{v}$  is

$$e^{-i\theta(\vec{v})} \equiv e^{-i\vec{v} \cdot [\vec{k}_3(t-\xi_{30}) + \vec{k}_2(t-\xi_{20}) + \vec{k}_1(t-\xi_{10})]} \quad (9)$$

If  $\theta(\vec{v}) = 0$  for all  $\vec{v}$ , then all molecules with different  $\vec{v}$  will radiate in phase, and the radiation intensity will be a maximum. This happens at  $t = t_e$  provided  $t_e \geq \xi_{30}$ , where

$$t_e = (\vec{k}_1 + \vec{k}_2 + \vec{k}_3) \cdot [\vec{k}_1 \xi_{10} + \vec{k}_2 \xi_{20} + \vec{k}_3 \xi_{30}] / |\vec{k}_1 + \vec{k}_2 + \vec{k}_3|^2 \\ \geq \xi_{30} \quad (10)$$

If  $t_e > \xi_{30}$ , the output is in the form of a pulse, known as photon echo. Generally, the photon echo will still appear if  $\theta(\vec{v})$  is always larger than zero, but has a minimum at  $t = t_m > \xi_{30}$ ; yet the echo intensity is greatly reduced if  $[\theta(\vec{v})]_{\min} \neq 0$ . When  $t_e$  (or  $t_m$ ) =  $\xi_{30}$ , the output appears as a modification on the third input pulse with a free induction decay tail.<sup>4</sup> No coherent output is expected if  $t_e(t_m) < \xi_{30}$ .

Formally, the density matrix  $\rho^{(3)}(t)$  of the molecular system should

be the average of  $\rho^{(3)}(\vec{v}, t)$  over the velocity distribution

$$\rho^{(3)}(t) = \int d\vec{v} n(\vec{v}) \rho^{(3)}(\vec{v}, t) \quad (11)$$

where  $n(\vec{v})$  is the velocity distribution function. In each term of  $\rho^{(3)}(\vec{v}, t)$ , the only factor depending on  $\vec{v}$  is  $\exp[i\theta(\vec{v})]$ , so that

$$\rho^{(3)}(t) \propto \int d\vec{v} n(\vec{v}) e^{i\theta(\vec{v})} \quad (12)$$

which has its maximum when  $\theta(\vec{v}) = 0$  at  $t = t_e \geq \xi_{30}$ . This may or may not happen depending on the problem, as we shall see later.

The other factors in Eq. (10) also carry physical significance. The phase factor  $\exp[i(\vec{k}_1 + \vec{k}_2 + \vec{k}_3) \cdot \vec{r}]$  indicates that the induced dipole oscillation has a wavevector  $\vec{k}_1 + \vec{k}_2 + \vec{k}_3$ . The dipole radiation from the collection of molecules is efficient only if the output has a wavevector  $\vec{k}(\omega)$  satisfying the phase matching condition  $\vec{k} = \vec{k}_1 + \vec{k}_2 + \vec{k}_3$ , as one would expect. The factor  $\exp[-\phi_{ps}(t - \xi_{30}) - \phi_{pr}(\xi_{30} - \xi_{20}) - \phi_{pm}(\xi_{20} - \xi_{10})]$  describes the decay of molecular excitation due to random perturbation if we assume that the frequency shifts due to random perturbation are negligible. The rest of the factors in Eq. (10) contribute to the intensity of the four-wave mixing output.

### C. Inhomogeneous Broadening in Solids

In solids, there is no Doppler effect due to molecular motion, but the resonant frequencies of molecules (or ions) are affected by local environment giving rise to inhomogeneous broadening. We can write

$$\omega_{ij} = \omega_{ij}^0 + \Delta\omega_{ij}(\alpha) \quad (13)$$

where  $\alpha$  represents a set of local parameters. We then have

$$\rho^{(3)}(t) = \int n(\alpha) \rho^{(3)}(\alpha, t) d\alpha \quad (14)$$

where  $n(\alpha)$  is the distribution function of  $\alpha$ , and  $\rho^{(3)}(\alpha, t)$  has the same expression as  $\rho^{(3)}(\vec{v}, t)$  except that in each term, all  $\omega_{ij}$ 's are replaced by  $\omega_{ij}^0$ , and  $\exp[-i\theta(\vec{v})]$  by  $\exp[-i\theta(\alpha)]$  which involves  $\Delta\omega_{ij}(\alpha)$ . For example,  $[\rho^{(3)}(\alpha, t)]_{(a)}$  can be obtained from the corresponding  $[\rho^{(3)}(\vec{v}, t)]_{(a)}$  in Eq. (8) with  $\omega_{ij}$  replaced by  $\omega_{ij}^0$  and  $\exp[-i\theta(\vec{v})]$  by

$$e^{-i\theta(\alpha)} = e^{-i[\Delta\omega_{ps} t - \Delta\omega_{rs} \xi_{30} - \Delta\omega_{mr} \xi_{20} - \Delta\omega_{pm} \xi_{10}]} \quad (15)$$

Again, in order to have the maximum coherent output, all molecules should radiate in phase. This requires  $\theta(\alpha) = 0$  for all  $\alpha$ , which is generally not possible. However, in a two-level system,  $\Delta\omega_{ps} = \Delta\omega_{rs} = \Delta\omega_{mr} = \Delta\omega_{pm}$ , we can have  $\theta(\alpha) = 0$  at  $t = t_e = \xi_{30} + \xi_{20} + \xi_{10}$ . More generally, if a particular local parameter  $\alpha_0$  dominates over the rest, and  $\Delta\omega_{ij} \approx \Delta\omega'_{ij}(\alpha_0)$ , then  $\theta(\alpha) = 0$  for all  $\alpha$  is approximately satisfied when

$$t = t_e = (\Delta\omega'_{rs} \xi_{30} + \Delta\omega'_{mr} \xi_{20} + \Delta\omega'_{pm} \xi_{10}) / \Delta\omega'_{ps} \quad (16)$$

Aside from this, the phase matching aspect and the decay of excitation due to random perturbation are the same as in the gas case.

#### D. Summary

Transient four-wave mixing with a given time order of the three input pulses is generally described by eight diagrams. The frequency of the output is  $\omega = \pm \omega_1 \pm \omega_2 \pm \omega_3$ , where "+" refers to absorption vertex on the left or emission vertex on the right in the diagram and "-" refers to emission vertex on the left or absorption vertex on the right. The wavevector of the induced third-order polarization is  $\vec{k}_s(\omega) = \pm \vec{k}_1(\omega_1) \pm \vec{k}_2(\omega_2) \pm \vec{k}_3(\omega_3)$  where the sign in front of  $\vec{k}_i(\omega_i)$  follows the sign of  $\omega_i$  in the above frequency relation. When  $\vec{k}(\omega) = \vec{k}_s(\omega)$ , the output is phase matched. An output pulse appears at  $t = t_e$  after the third input pulse when all molecules radiate in phase through rephasing of the dephased molecular excitation. Assuming the spectral widths of input pulses being much larger than the homogeneous and inhomogeneous widths, we find  $t_e$  given by Eqs. (10) and (16) for gas and solid respectively. The intensity of the output pulse is proportional to  $|\rho^{(3)}(t_e)|^2$ .

### III. Specific Cases

We now use the results of the previous section to analyze the various cases of transient four-wave mixing in effectively two-, three-, and four-level systems. We will not try to discuss all possible cases, but will focus the attention to cases where all input pulses induce resonant or near-resonant excitations in the medium, i.e., the triply resonant cases.

#### A. Two-Level System

We consider the special case where all the input pulses have the same frequency  $|\omega_1| = |\omega_2| = |\omega_3| \equiv \omega \approx \omega_{10}$  as shown in Fig. 2, but the wavevectors can be all different. In deriving  $\rho^{(3)}(t)$  for this case, only

the resonant terms will be kept. They come from the diagrams in Fig. 1a and 1d with the  $\omega_2$  wavy line changed to a negative slope to indicate a  $(-\omega)$  interaction, and Fig. 1f and 1g with the  $\omega_1$  wavy line changed to a negative slope. We summarize the results in Table 1, where line 1 shows the diagrams, line 2 gives the possible phase matching configurations related to the diagrams (note that the wavevectors do not have to be coplanar), line 3 specifies  $t_e$  for those cases where  $\theta(\vec{v}$  or  $\alpha) = 0$  can be satisfied for gas and solid respectively, and line 4 gives  $\rho^{(3)}(t_e)$  which corresponds to the maximum output in transient four-wave mixing. As we mentioned earlier, it is possible to have coherent output of reduced amplitude if  $\theta(\vec{v}$  or  $\alpha)$  is a minimum at  $t = t_m \geq \xi_{30}$ , but we shall not discuss such cases here although the extension is quite straightforward.<sup>4</sup>

The results in Table 1 reproduce the conditions for three-pulse stimulated echoes<sup>7</sup> in two-level systems derived by Fujita et al.<sup>8</sup> using the non-perturbative method. In the perturbation limit, the latter also yields the same echo amplitude as the one we have obtained. As can be easily seen, cases (a), (b), and (f) in Table 1, whenever possible, can generate a backward echo, while cases (d) and (e) generate the forward stimulated echo with  $\delta \approx 0$ .

It is interesting to see that the results here can also be related to the two-pulse photon echoes.<sup>7</sup> We simply let the second and third input pulses merge into one with  $\xi_{20} = \xi_{30}$ ,  $\vec{k}_2 = \vec{k}_3$ , and  $\vec{\epsilon}_2 = \vec{\epsilon}_3$ . The two-pulse echo can occur only for case (d) or (e) in Table 1. For perfect phase matching, collinear geometry must be used. The echo appears at  $t_e - \xi_{30} = \xi_{20} - \xi_{10}$ ; in other words, the echo pulse is separated from the second pulse by the same duration as the second pulse from the first

pulse. The echo amplitude decays with  $\exp[-2\phi_{10}(\xi_{20} - \xi_{10})]$ . These are all results familiar in two-pulse photon echoes in two-level systems. One can also imagine that the first and second input pulses may merge into one with  $\xi_{10} = \xi_{20}$ ,  $\vec{k}_1 = \vec{k}_2$ , and  $\vec{e}_1 = \vec{e}_2$ . In this case,  $t_e = \xi_{30}$ , and the output pulse overlaps with and modifies the input pulse at  $\xi_{30}$ . This can be illustrated by examining  $\rho^{(3)}(t)$  assuming  $\omega = \omega_{10}$  in a gas medium

$$\begin{aligned} \rho^{(3)}(t) \propto & e^{-i\omega_{10}t - \phi_{10}(t - \xi_{30})} \int d\vec{v} n(\vec{v}) e^{i\vec{k}_s \cdot \vec{v}(t - t_e)} \\ & \times \left[ e^{-\phi_{00}(\xi_{30} - \xi_{20})} + e^{-\phi_{11}(\xi_{30} - \xi_{20})} \right] \int_{-\infty}^t d\xi_3 A_3(\xi_3). \end{aligned} \quad (17)$$

It is seen that the output is in the form of a free induction decay characterized by the time-varying function

$$\left[ \int_{-\infty}^t d\xi_3 A_3(\xi_3) \right] e^{-i\omega_{10}t - \phi_{10}(t - \xi_{30})} \int d\vec{v} n(\vec{v}) e^{i\vec{k}_s \cdot \vec{v}(t - t_e)}$$

and its amplitude decreases with the pulse separation time  $(\xi_{30} - \xi_{20})$  following  $\left[ e^{-\phi_{00}(\xi_{30} - \xi_{20})} + e^{-\phi_{11}(\xi_{30} - \xi_{20})} \right]$ . Physically, the first of the two input pulses pumps the population, and the second probes the population decay. This corresponds to the transient laser-induced saturation or birefringence effect. The output is a transient response to the probe pulse and the population excitation of the first input pulse. If the probe pulse is tunable with  $\omega' \approx \omega$ , then the effect here is related to the well known transient saturation or polarization spectroscopy.<sup>9</sup>

### B. Three-Level System

We consider the three processes shown in Fig. 3 with the frequencies of the input pulses being  $\omega_a = |\omega_{10}|$  and  $\omega_b = |\omega_{21}|$ , and  $|1\rangle$  is assigned to be the common level for the two resonant transitions. The problem has been discussed earlier by others using the usual nonperturbative approach.<sup>4,5,10</sup> For each process in Fig. 3, there are several distinct time orderings of the three input pulses leading to different physical cases. For Fig. 3a, there are three different cases: (A) an  $\omega_a$  pulse is followed by two  $\omega_b$  pulses; (B) an  $\omega_a$  pulse is followed by an  $\omega_b$  pulse and then an  $\omega_a$  pulse; (C) two  $\omega_a$  pulses are followed by an  $\omega_b$  pulse. We have again in mind that in deriving the output of transient four-wave mixing, only the resonant terms in  $\rho^{(3)}(t)$  are kept. The results for the three different cases of the process in Fig. 3a are summarized in Table 2. It is seen that the so-called sum-frequency trilevel echo<sup>11</sup> in case (A) has frequency  $\omega_a$ , while those in cases (B) and (C) have frequency  $\omega_b$ . The pulse excitations in (A) and (B) are all coherent excitations between pairs of states, and therefore the echo amplitude decays depend only on the dephasing rates between the pairs of states. Case (C) involves population excitation, and the echo amplitude decay depends also on the population relaxation.

Two-pulse echoes are also possible in three-level systems, corresponding to the special case of  $\xi_{20} = \xi_{30}$  in the general three-pulse case. With  $\xi_{10} = \xi_{20}$  and  $\vec{k}_1 = \vec{k}_2$ , the output pulse appears overlapping with the input pulse at  $\xi_{30}$  with a free-induction decay tail. This corresponds to the case of transient three-level laser-induced absorption or birefringence. The  $\omega_a$  pulse at  $\xi_{10} = \xi_{20}$  pumps the population into  $|1\rangle$ . The

probe pulse probes the population in  $|1\rangle$  at a later time  $\xi_{30}$ , and the output appears in the form of a free induction decay superposed on the probe pulse.<sup>9</sup>

The process in Fig. 3b is essentially the same as that in Fig. 3a, except that  $|2\rangle$  is now below  $|1\rangle$ . Therefore, the results in Table 2 for Fig. 3a are also valid for Fig. 3b if we replaced  $\omega_b$  by  $-\omega_b$  and the respective wavevectors  $\vec{k}_i(\omega_b)$  by  $-\vec{k}_i(\omega_b)$ . Note that  $[\rho^{(3)}(-\omega_b, t)]^+ = \rho^{(3)}(\omega_b, t)$ .

The process in Fig. 3c is more interesting since the common level for the two transitions is now the ground level. Six different physical cases from six different time orderings of the  $\omega_a$  and  $\omega_b$  input pulses are possible. Three are the same as cases (A), (B), and (C) for Figs. 3a and 3b. The other three are similar cases with  $\omega_a$  and  $\omega_b$  interchanged. We will not spell out the results completely here, but simply present the diagrams for the different cases in Fig. 4 and the corresponding expressions of  $\rho^{(3)}(t_e)$  in the following.

$$\begin{aligned} \rho^{(3)}(\omega_a, t_e) = & - \left( \frac{1}{2i\hbar} \right)^3 e^{i(\vec{k}_s \cdot \vec{r} - \omega_0 t_e)} \langle 0 | \vec{\mu} \cdot \hat{e}_1 | 1 \rangle \langle 1 | \vec{\mu} \cdot \hat{e}_2 | 2 \rangle \langle 2 | \vec{\mu} \cdot \hat{e}_3 | 1 \rangle \\ & \times ( |0\rangle \rho_{11} \langle 1| ) e^{-[\phi_{01}(t_e - \xi_{30}) + \phi_{20}(\xi_{30} - \xi_{20}) + \phi_{01}(\xi_{20} - \xi_{10})]} \\ & \times \int_{-\infty}^t d\xi_3 e^{i(\omega_{21} - \omega_b)\xi_3} A_3(\xi_3) \int_{-\infty}^{\xi_3} d\xi_2 e^{-i(\omega_{21} - \omega_b)\xi_2} A_2^*(\xi_2) \\ & \times \int_{-\infty}^{\xi_2} d\xi_1 e^{i(\omega_{01} - \omega_a)\xi_1} A_1(\xi_1) \end{aligned} \quad (18A)$$

$$\rho^{(3)}(\omega_b, t_e) = - \left( \frac{1}{2i\hbar} \right)^3 e^{i(\vec{k}_s \cdot \vec{r} - \omega_{21} t_e)} \langle 2 | \vec{\mu} \cdot \hat{e}_2 | 1 \rangle \langle 1 | \vec{\mu} \cdot \hat{e}_1 | 0 \rangle \langle 0 | \vec{\mu} \cdot \hat{e}_3 | 1 \rangle$$

cont'd

$$\begin{aligned}
& \times (|2\rangle\rho_{11}\langle 1|) e^{-[\phi_{21}(t_e - \xi_{30}) + \phi_{20}(\xi_{30} - \xi_{20}) + \phi_{01}(\xi_{20} - \xi_{10})]} \\
& \times \int_{-\infty}^t d\xi_3 e^{i(\omega_{01} - \omega_a)\xi_3} A_3(\xi_3) \int_{-\infty}^{\xi_3} d\xi_2 e^{i(\omega_{21} - \omega_b)\xi_2} A_2(\xi_2) \\
& \times \int_{-\infty}^{\xi_2} d\xi_1 e^{-i(\omega_{01} - \omega_a)\xi_1} A_1^*(\xi_1) \tag{18B}
\end{aligned}$$

$$\begin{aligned}
\rho^{(3)}(\omega_b, t_e) &= - \left( \frac{1}{2i\hbar} \right)^3 e^{i(\vec{k}_s \cdot \vec{r} - \omega_{21} t_e)} |2\rangle\rho_{11}\langle 1| \\
& \times e^{-[\phi_{21}(t_e - \xi_{30}) + \phi_{11}(\xi_{30} - \xi_{20}) + \phi_{01}(\xi_{20} - \xi_{10})]} \\
& \times \langle 2 | \vec{\mu} \cdot \hat{e}_3 | 1 \rangle \int_{-\infty}^t d\xi_3 e^{i(\omega_{21} - \omega_b)\xi_3} A_3(\xi_3) \\
& \times \left[ \langle 1 | \vec{\mu} \cdot \hat{e}_2 | 0 \rangle \langle 0 | \vec{\mu} \cdot \hat{e}_1 | 1 \rangle \int_{-\infty}^{\xi_3} d\xi_2 e^{-i(\omega_{01} - \omega_a)\xi_2} A_2^*(\xi_2) \right. \\
& \times \left. \int_{-\infty}^{\xi_2} d\xi_1 e^{i(\omega_{01} - \omega_a)\xi_1} A_1(\xi_1) + \text{complex conjugate} \right]. \tag{18C}
\end{aligned}$$

The expressions of  $\rho^{(3)}(t_e)$  for cases (D), (E), and (F) are obtained by interchanging  $\omega_a$  and  $\omega_b$  in Eqs. (18A), (18B), and (18C). Photon echoes related to the process of Fig. 3c are called inverted-difference-frequency trilevel echoes.<sup>4</sup>

### C. Four-Level System

Consider first the four-level system with two basically different processes shown in Fig. 5. The three input pulses with frequencies  $\omega_a$ ,  $\omega_b$ , and  $\omega_c$  are triply resonant with the four-level system. Photon echoes in a four-level system with three input frequencies have been discussed earlier with the nonperturbative method.<sup>4,12</sup>

In Fig. 5a,  $\omega_a \approx \omega_{10}$ ,  $\omega_b \approx \omega_{10'}$ , and  $\omega_c \approx \omega_{1'0'}$ . The only possible time order of a triply resonant excitation is indicated in the diagram of Table 3. The results derived from the diagram are also listed in Table 3. In Fig. 5b,  $\omega_a \approx \omega_{10}$ ,  $\omega_b \approx \omega_{10'}$ , and  $\omega_c \approx \omega_{1'0}$ . Three possible time orderings of the process are as follows: (A)  $\omega_a$  pulse followed successively by  $\omega_b$  and  $\omega_c$  pulses; (B)  $\omega_a$  pulse followed successively by  $\omega_c$  and then  $\omega_b$  pulses; (C)  $\omega_c$  pulse followed successively by  $\omega_a$  and  $\omega_b$  pulses. They correspond to three different physical cases. The diagrams and the corresponding results for the three cases are given in Table 4. For the processes in both Fig. 5a and Fig. 5b, three-pulse photon echo can occur. Since all excitations are coherent excitations between pairs of states, the decay of the echo amplitude depends only on the dephasing rates between appropriate pairs of states.

A variation of the four-level system of Fig. 5 is shown in Fig. 6. The  $\langle 0' |$  level is now above the  $\langle 1 |$  and  $\langle 1' |$  levels. The results of Table 3 can be used for the process in Fig. 6a if we replace  $\omega_b$  and  $\omega_c$  by  $-\omega_b$  and  $-\omega_c$ , and  $\vec{k}_i(\omega_b)$  and  $\vec{k}_j(\omega_c)$  by  $-\vec{k}_i(\omega_b)$  and  $-\vec{k}_j(\omega_c)$ . The results of Table 4 can be used for Fig. 6b with  $\omega_b$  replaced by  $-\omega_b$  and  $\vec{k}_i(\omega_b)$  by  $-\vec{k}_i(\omega_b)$ . Again, note that  $\rho^{(3)}(\omega, t) = [\rho^{(3)}(-\omega, t)]^+$ .

Another variation of Fig. 5a is shown in Fig. 7. The results of Table 3 also apply to this case if we replace  $\omega_b$  by  $-\omega_b$  and  $\vec{k}_i(\omega_b)$  by  $-\vec{k}_i(\omega_b)$ .

Finally, we consider a special case of transient four-wave mixing in a four-level system in which there are levels connected only by population relaxation, but not by coherent excitation. An example is shown in Fig. 8a. Physically, the first two input pulses at  $\omega_a$  with wavevectors

$\vec{k}_1$  and  $\vec{k}_2$  pumps population into  $\langle 1|$  and forms a population grating. Through relaxation, the population grating is transferred to  $\langle 1'|$ . The third input pulse at  $\omega_b$  then coherently excites the system from  $\langle 1'|$  to  $\langle 2|$  and produces a stimulated photon echo at  $\omega_b$ . We use the diagrams in Fig. 8b to represent this transient phenomenon. The dotted lines in the diagrams describe the relaxation of the excited population  $\rho_{11}^{(2)}$  in  $|1\rangle$  to  $\rho_{1'1'}^{(2)}$  in  $|1'\rangle$ . We can easily show that the conditions for observing a coherent transient output are the same as those given in Table 2c. If we assume  $\rho_{1'1'}^{(2)} = \alpha \rho_{11}^{(2)}$ , where  $\alpha$  is a proportional constant, then the echo amplitude is still given by  $\rho^{(3)}(\omega_b, t_e)$  in Table 2(C) with a simple substitution of  $\langle 2|\vec{\mu} \cdot \hat{e}_3|1\rangle e^{-\phi_{21}(t_e - \xi_{30})} \int_{-\infty}^t e^{i(\omega_{21} - \omega_b)\xi_3} A_3(\xi_3) d\xi_3$  by  $\langle 2|\vec{\mu} \cdot \hat{e}_3|1'\rangle e^{-\phi_{21'}(t_e - \xi_{30})} \int_{-\infty}^t e^{i(\omega_{21'} - \omega_b)\xi_3} A_3(\xi_3) d\xi_3$ . When  $\xi_{10} = \xi_{20}$  as the two  $\omega_a$  pulses merge into one, the output should again appear as a free induction decay superposed on the  $\omega_b$  probe pulse. This actually corresponds to the case of collision-induced transient saturation spectroscopy.

#### IV. Discussion

The main application of transient four-wave mixing is to study the decays of various excitations in a medium. Both the dephasing rate of coherent excitation between any pair of states and the population relaxation rate of a given state can be measured. In an effective two-level system, for example, the dephasing rate can be obtained from the two-pulse photon echo measurement, while the population relaxation can be measured by transient saturation spectroscopy. Three-pulse echoes in a two-level system in general are connected to both coherent excitation and population excitation. Its decay is governed by both the dephasing rate and

the population relaxation.

In an effective three-level system, the dephasing rates between any pair of states and the population relaxation rate of the common level for two different transitions can be separately determined by a series of photon echo measurements. Take Fig. 3a as an example. Examination of the expressions of  $\rho^{(3)}(t_e)$  for the three cases in Table 2 shows the following possibilities. First, using the two-pulse echo arrangement with  $\xi_{20} = \xi_{30}$ , we can determine  $\phi_{10}$  from the  $\omega_a$  echo measurement of case (A), and then  $\phi_{21}$  from the  $\omega_b$  echo measurement of case (B). Next, the general three-pulse echo measurement of either case (A) or case (B) allows the determination of  $\phi_{20}$ . Finally, the photon echo measurement or the transient saturation spectroscopic measurement ( $\xi_{10} = \xi_{20}$ ) of case (C) can be used to determine the population relaxation rate  $\phi_{11}$  of the common level  $|1\rangle$ . In order to find the population relaxation rates  $\phi_{22}$  and  $\phi_{00}$ , processes schematically shown in Figs. 3b and 3c should be used. Similarly, all the relaxation rates in a four-level system can be determined by a series of appropriate transient four-wave mixing experiments. It is particularly interesting to note that dephasing rates between two excited states or between two states not directly connected by electric dipole transition can be obtained from such measurements. With proper polarization arrangement, it is also possible to deduce the relaxation rates involving only one of the several degenerate states in the same level. We should mention that actually, singly resonant transient four-wave mixing can also be used, perhaps more straightforwardly, to measure dephasing rates between selective pairs of states. Transient coherent antiStokes Raman scattering is an example.<sup>13</sup> Transient detection by wave mixing of

a coherent excitation is another example. Triply resonant four-wave mixing, however, is capable of yielding a much larger signal.

We have assumed that the imaginary part of  $\phi_{ij}$  is negligible so that  $\phi_{ij} \approx \gamma_{ij}$ . In a gas medium, we can write  $\gamma_{ij} = \gamma_{ij}^c + \gamma_{ij}^s$ , where  $\gamma_{ij}^c$  is the dephasing rate due to atomic or molecular collisions, and  $\gamma_{ij}^s$  is due to single-atom radiative decay.<sup>14</sup> Since  $\gamma_{ij}^c \propto \sigma_{ij} p$  with the proportional constant known, measurement of  $\gamma_{ij}$  as a function of the foreign gas pressure  $p$  enables us to determine in principle  $\gamma_{ij}^s$  and the collision cross-section  $\sigma_{ij}$ .<sup>4-6</sup> In the above discussion, however, we have assumed that the atomic velocity is not affected by collisions. This is of course not true in general. Velocity changing collisions between the excitation pulses increase the decay of coherent signal because of the increased velocity dephasing.<sup>4,5</sup> The effect is more significant for longer time separations between pulses, and has already been experimentally demonstrated.<sup>15</sup> For sufficiently short pulse separation, the effect is negligible.

In a solid, if Eq. (17) for  $t_e$  is valid, then by measuring  $t_e$  as a function of  $\xi_{30} - \xi_{20}$  and  $\xi_{20} - \xi_{10}$  for various photon echo cases in a three- or four-level system, the inhomogeneous broadening parameters  $\Delta\omega'_{ij}$  for different pairs of states can be deduced. This is interesting since the same information cannot be easily obtained by other methods.

The echo pulse in a gas medium is described by  $\rho^{(3)}(t)$  given in Eq. (12) or (13) with  $t \sim t_e$ . Its shape results from rephasing and then dephasing of dipole radiation from molecules with different velocities as  $t$  varies around  $t_e$  or ( $t_m$  if  $\theta(\vec{v})$  is always positive but has a minimum), and is mainly determined by  $\theta(\vec{v}, t)$  in the integral in Eq. (13), which can also be written as

$$\rho^{(3)}(t) \propto R = \int_{-\infty}^{\infty} d\vec{v} n(\vec{v}) e^{-i\vec{v} \cdot \vec{k}_s (t-t_e)} \quad (19)$$

Thus, if  $n(\vec{v})$  is known, the echo pulse shape can in principle be calculated. In the case of solids, we have, following Eqs. (15) and (16)

$$\begin{aligned} R &= \int_{-\infty}^{\infty} d\alpha n(\alpha) e^{-i\Delta\omega_{ps}(\alpha)(t-t_e)} \\ &= \int_{-\infty}^{\infty} d(\Delta\omega_{ps}) n(\Delta\omega_{ps}) e^{-i\Delta\omega_{ps}(t-t_e)} \end{aligned} \quad (20)$$

The echo pulse shape is determined by the distribution of the inhomogeneous broadening of the radiative transition.

So far, we have assumed in Sec. III and in the above discussion that the exciting pulses are sufficiently short so that the approximation in Eq. (8) is valid. This is equivalent to saying that the spectral widths of the exciting pulses are much larger than both the homogeneous linewidths and the Doppler widths. However, if the exciting laser linewidths are comparable to or smaller than the Doppler widths, then only a fraction of molecules with velocities in a certain region will be excited. Yet the transient four-wave mixing should still exist even though its intensity is reduced. The velocity dephasing time increases and the echo pulse is expected to become longer. The same is true for solids if the exciting laser linewidths are smaller than the inhomogeneously broadened widths, so that only a fraction of ions effectively participates in transient four-wave mixing.

As we have seen, transient four-wave mixing can predict all the pho-

ton echo phenomena known from the usual treatment. Being a perturbative treatment, however, the theoretical derivation of transient four-wave mixing is perhaps simpler, more transparent, and more easily generalized. For example, we can treat the case of three overlapping input pulses and the case of three separated pulses on the same footing, although they may yield different coherent transient phenomena.

The treatment of transient four-wave mixing here can also be readily extended to transient  $n$ -wave mixing. Thus, for example, without going through any detailed calculation, one can predict all the important characteristics of the photon echoes from an  $m$ -level system with  $n$  excitation pulses. Other coherent transient optical effects involving multiple resonant excitation pulses are also possible.

This work was supported by the Director, Office of Energy Research, Office of Basic Energy Sciences, Materials Sciences Division of the U.S. Department of Energy under Contract No. W-7405-ENG-48.

## References

1. See, for example, the brief review by N. Bloembergen, in Laser Spectroscopy IV, edited by H. Walther and K. W. Rothe (Springer-Verlag, Berlin, 1979), p.340.
2. S. A. J. Druet, J-P. E. Taran, and Ch. J. Borde, J. Phys. (Paris) 40, 841 (1979); 41, 183 (1980).
3. J-L. Oudar and Y. R. Shen, Phys. Rev. A 22, 1141 (1980).
4. T. M. Mossberg, R. Kachru, S. R. Hartmann, and A. M. Flusberg, Phys. Rev. A 20, 1976 (1979).
5. R. Brewer, in Nonlinear Spectroscopy, Proc. International School of Physics, Course 64, edited by N. Bloembergen (North-Holland Publishing Co., Amsterdam, 1977), p.87.
6. T. K. Yee and T. K. Gustafson, Phys. Rev. A 18, 1597 (1978).
7. S. R. Hartmann, in Quantum Optics, Proc. of the International School of Physics, Enrico Fermi, Course 42, edited by R. J. Glauber (Academic Press, NY, 1969), p.532.
8. M. Fujita, H. Nakasuka, H. Nakanishi, and M. Matsuoka, Phys. Rev. Lett. 42, 974 (1979).
9. T. W. Hansch, Physics Today 30, #5, 34 (1977).
10. R. G. Brewer and E. L. Hahn, Phys. Rev. A 11, 1641 (1975).
11. T. Mossberg, A. Flusberg, R. Kachru, and S. R. Hartmann, Phys. Rev. Lett. 39, 1523 (1977).
12. C. V. Heer and R. L. Sutherland, Phys. Rev. A 19, 2026 (1979).
13. R. R. Alfano and S. L. Shapiro, Phys. Rev. Lett. 26, 1247 (1971);  
D. von der Linde, A. Laubereau, and W. Kaiser, Phys. Rev. Lett. 27,

802 (1971).

14. A. Omont, E. W. Smith, and J. Cooper, *Astrophys. J.* 175, 185 (1972).
15. T. Mossberg, A. Flusberg, R. Kachru, and S. R. Hartmann, *Phys. Rev. Lett.* 42, 1665 (1979).

## Figure Captions

- Fig. 1 Eight possible diagrams for transient four-wave mixing with a given time order for the three input waves.
- Fig. 2 Resonant four-wave mixing in a two-level system with  $\omega \sim \omega_{10}$ .
- Fig. 3 Resonant four-wave mixing in three possible three-level systems.
- Fig. 4 Diagrams for the six possible cases of resonant four-wave mixing in Fig. 3c.
- Fig. 5 Resonant four-wave mixing in a four-level system.
- Fig. 6 Resonant four-wave mixing in a four-level system.
- Fig. 7 Resonant four-wave mixing in a four-level system.
- Fig. 8 Transient four-wave mixing in a system with two levels connected only by population relaxation.

## Table Captions

- Table 1 Summary of results for the transient four-wave mixing process in Fig. 2.
- Table 2 Summary of results for the transient four-wave mixing process in Fig. 3.
- Table 3 Summary of results for the transient four-wave mixing process in Fig. 5a.
- Table 4 Summary of results for the transient four-wave mixing processes in Fig. 5b.

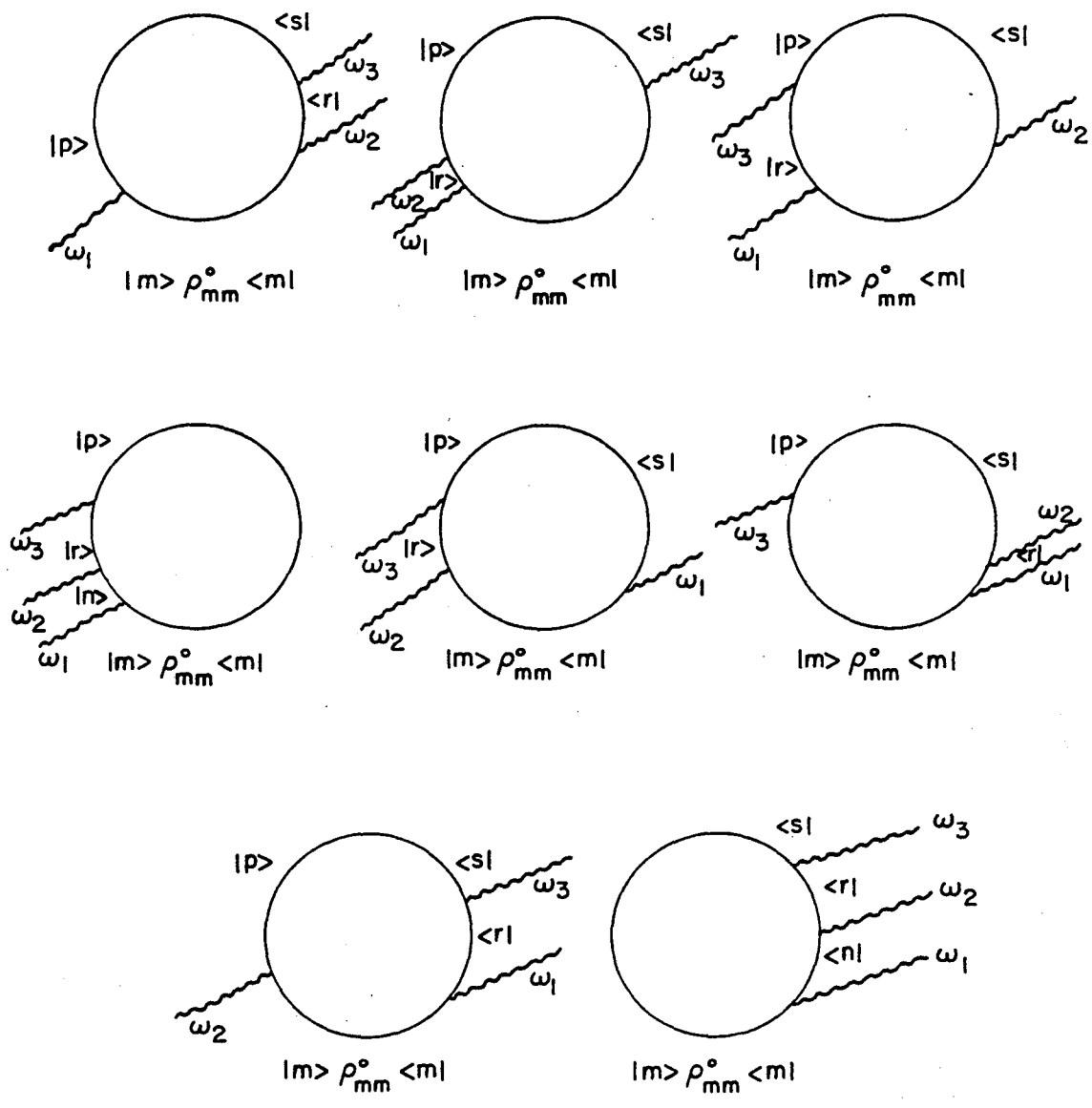
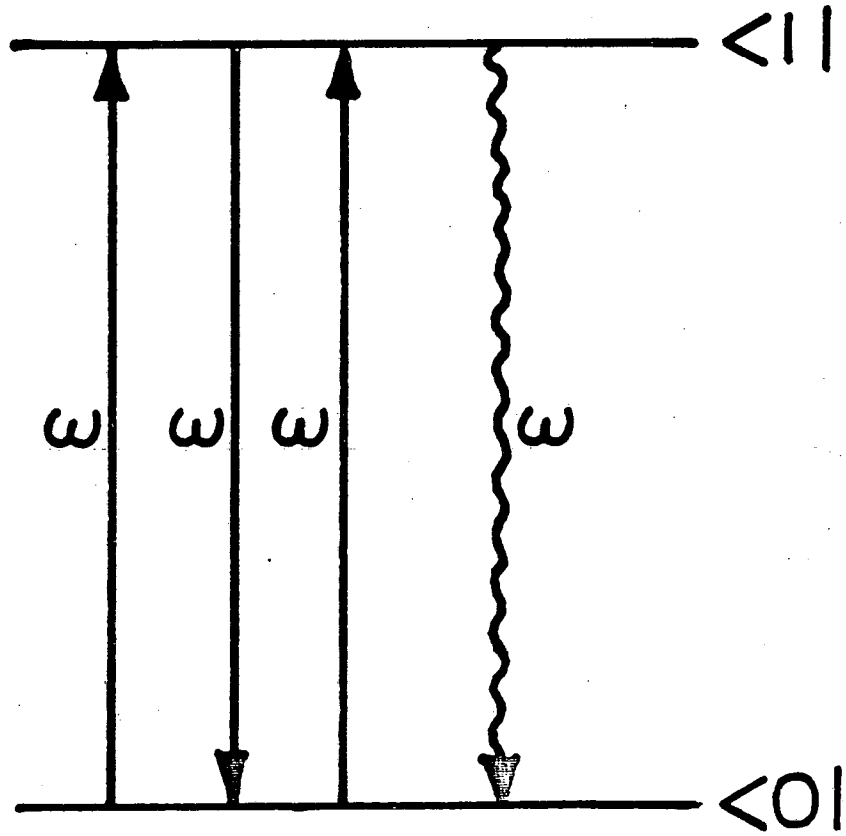


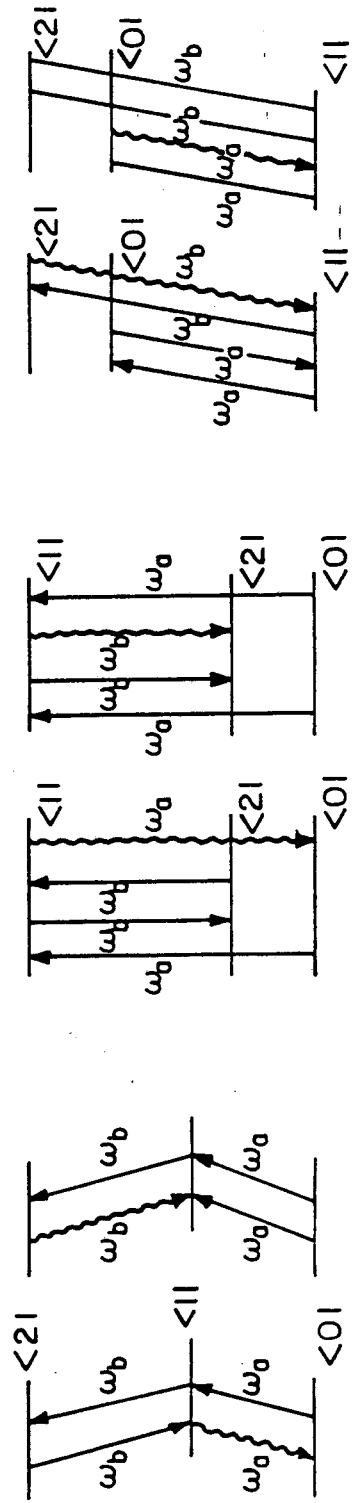
Fig. 1

XBL 8110-11700



XBL 8110-11701

Fig. 2



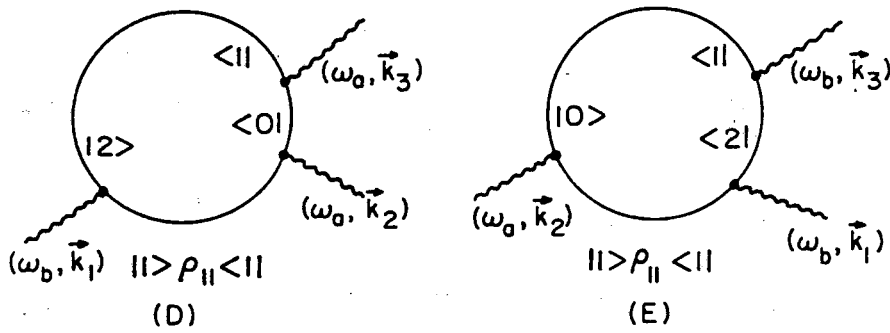
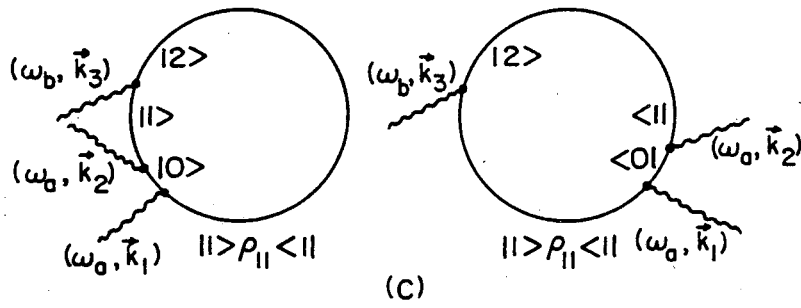
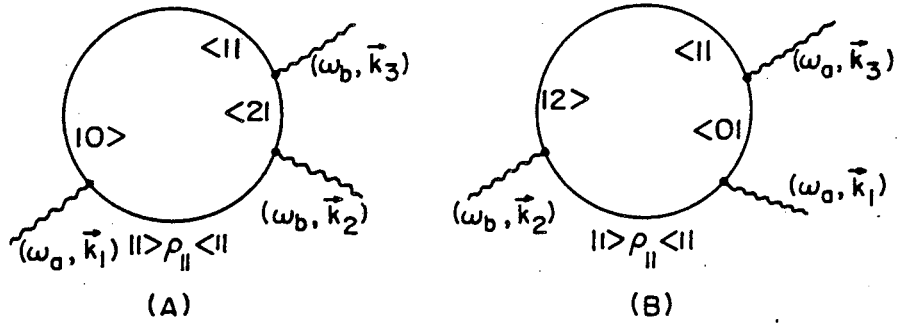
(a)

(b)

(c)

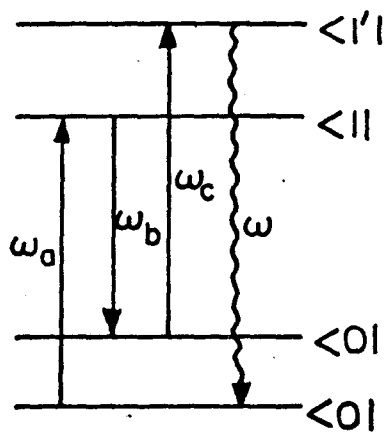
XBL 8110-11702

FIG. 3

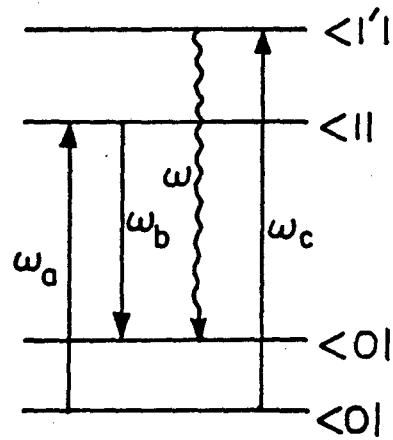


(F)  
Fig. 4

XBL 8110-11703



(a)



(b)

XBL 8110-11704

Fig. 5

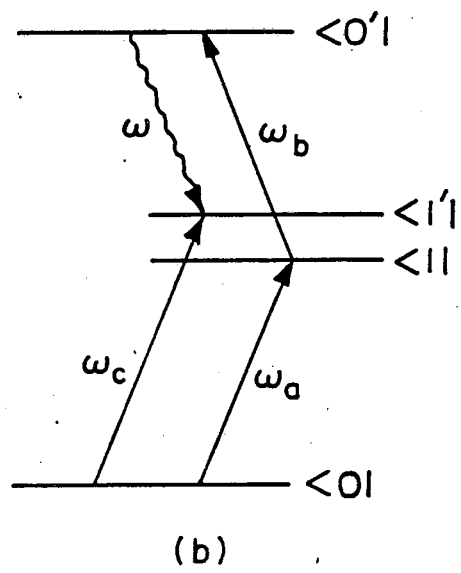
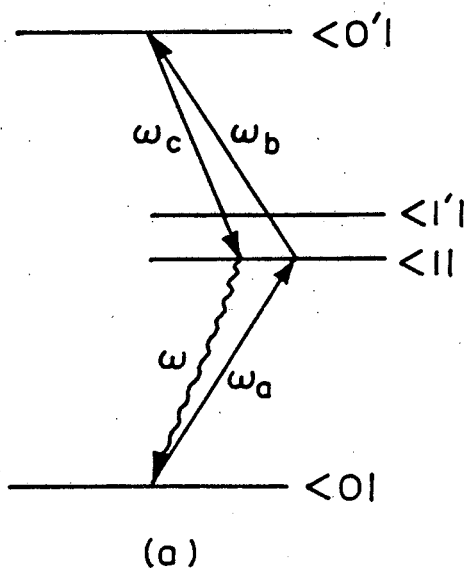
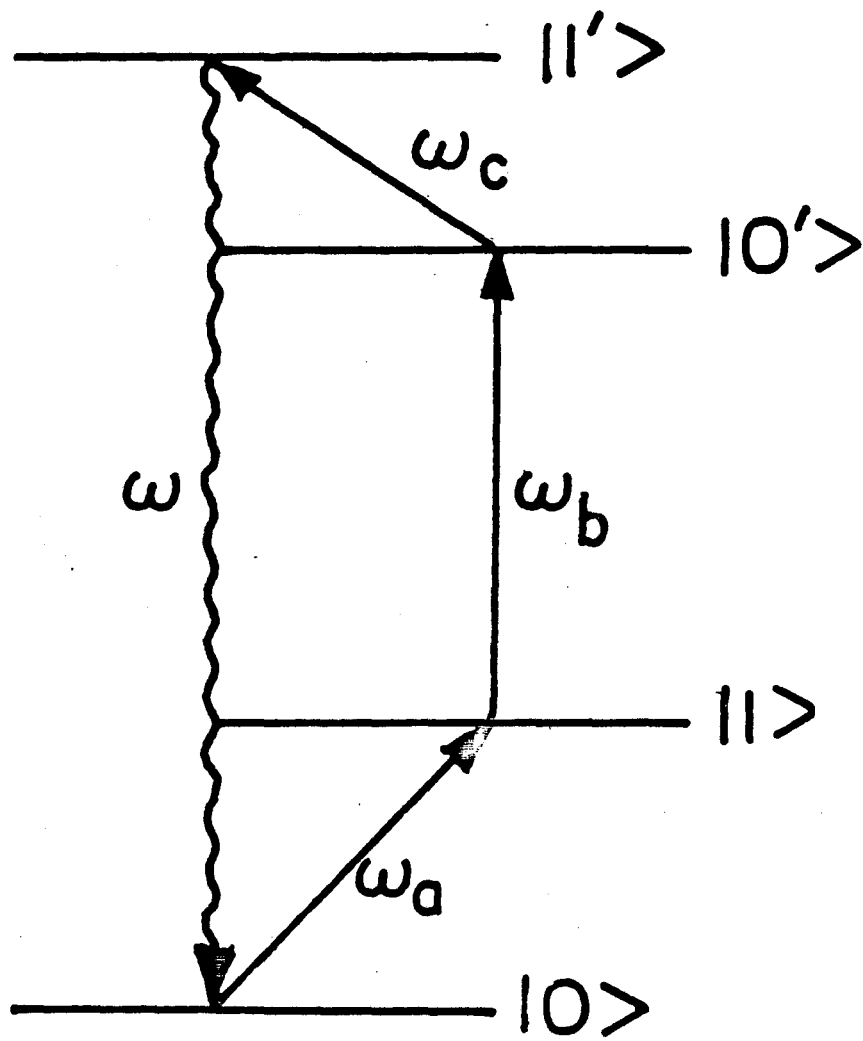


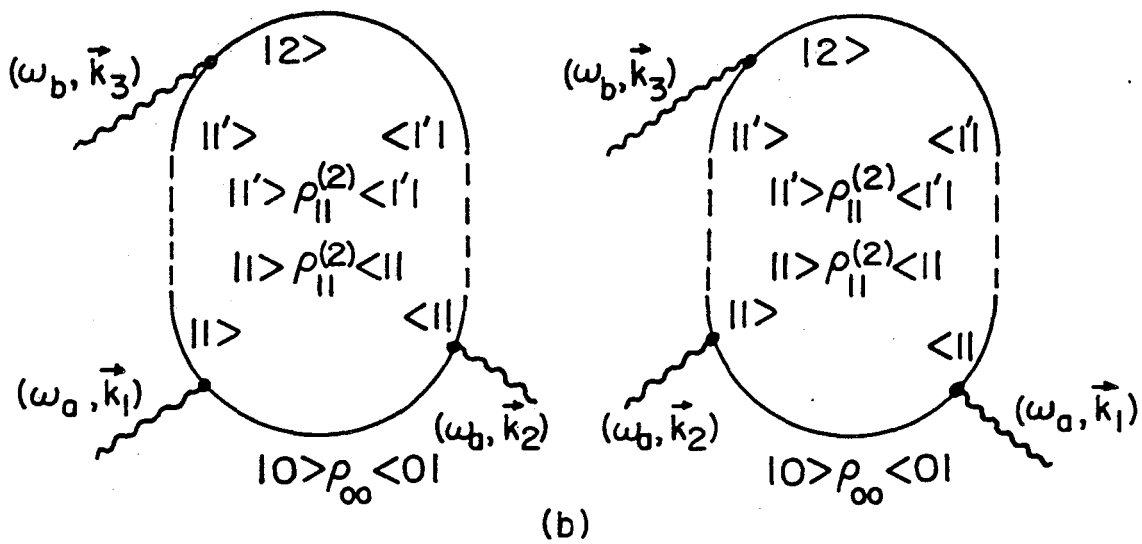
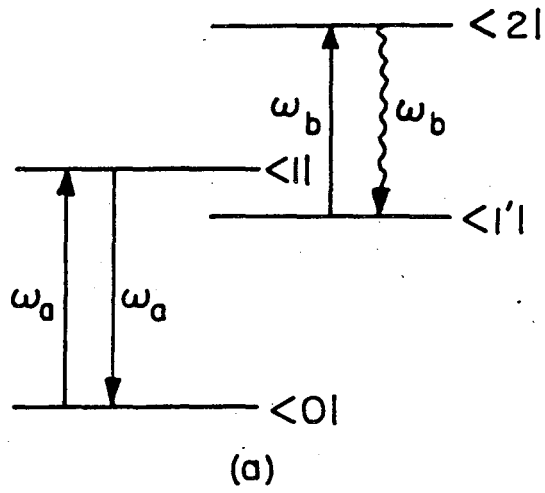
Fig. 6

XBL 8110-11705



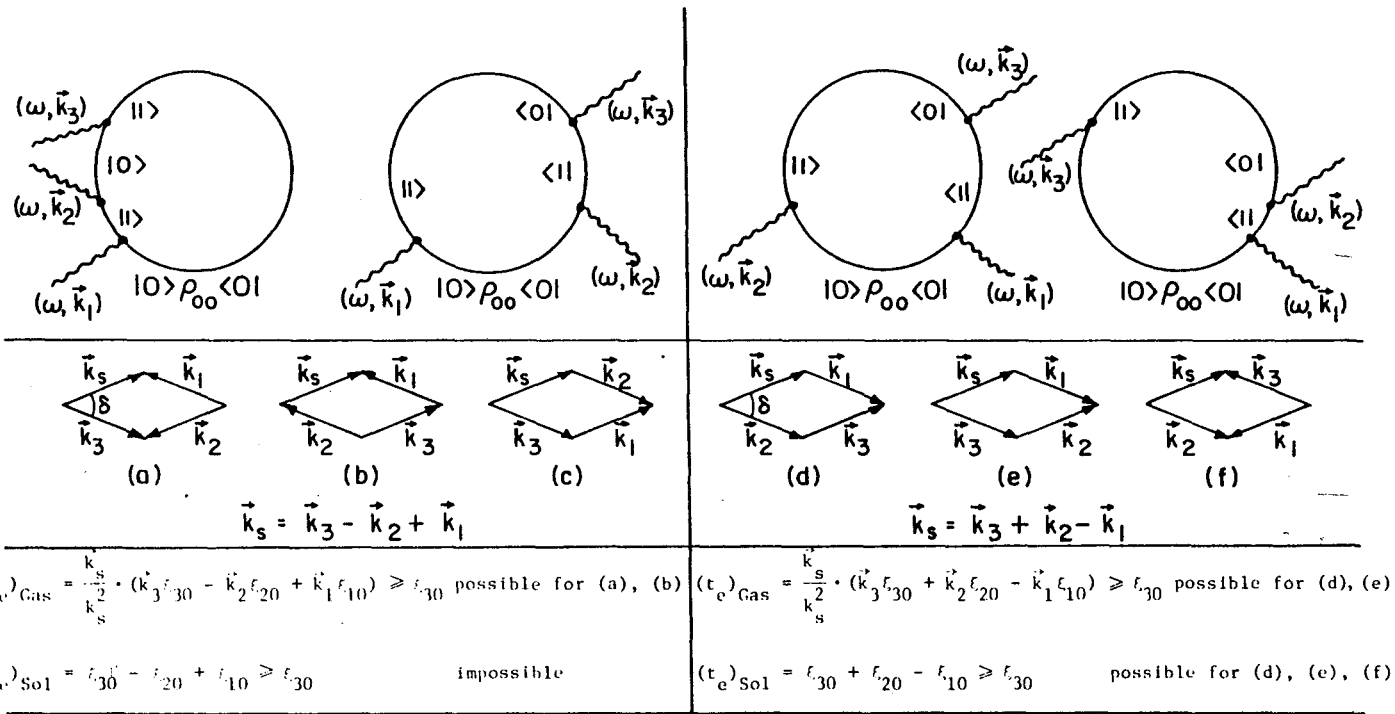
XBL 8110-11706

Fig. 7



XBL 8110-11707

Fig. 8

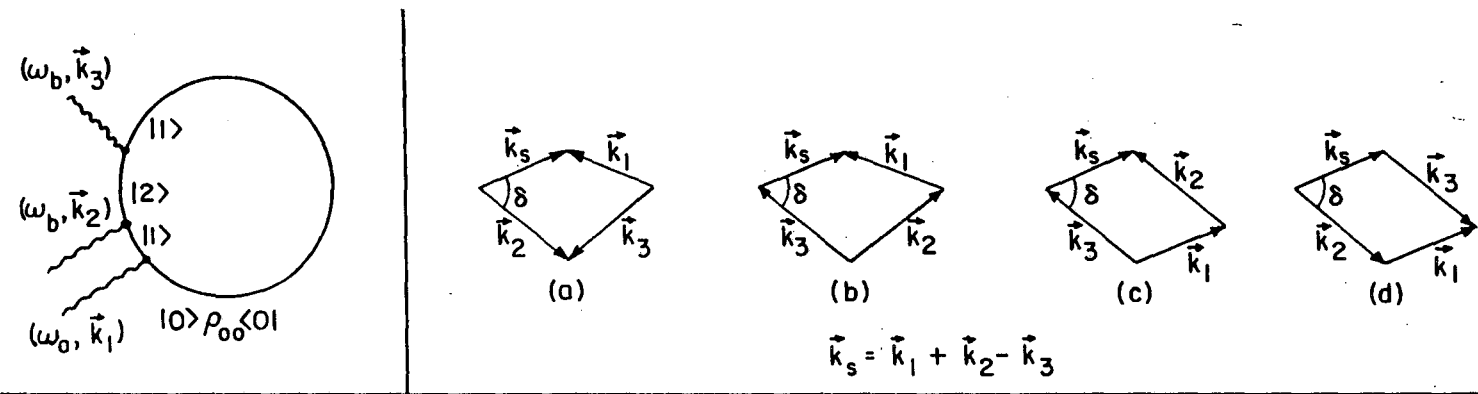


$$u^{(3)}(t_e) = - \left( \frac{1}{2i\hbar} \right)^3 e^{-i\omega t_e} \langle 1 | \rho_{00} \rangle e^{-\phi_{10}(t_e - \epsilon_{30} + \epsilon_{20} - \epsilon_{10})} \left[ e^{-\phi_{00}(\epsilon_{30} - \epsilon_{20})} + e^{-\phi_{11}(\epsilon_{30} - \epsilon_{20})} \right]$$

$$\begin{aligned} & \cdot \left\langle 1 | \vec{u} \cdot \hat{e}_3 | 0 \rangle \langle 0 | \vec{u} \cdot \hat{e}_2 | 1 \rangle \langle 1 | \vec{u} \cdot \hat{e}_1 | 0 \rangle e^{i(\vec{k}_3 - \vec{k}_2 + \vec{k}_1) \cdot \vec{r}} \int_{-\infty}^t e^{d\epsilon_3 \Lambda_3(\epsilon_3)} e^{i(\omega_{10} - \omega)\epsilon_3} \\ & \cdot \int_{-\infty}^{\epsilon_3} d\epsilon_2 \Lambda_2^*(\epsilon_2) e^{-i(\omega_{10} - \omega)\epsilon_2} \int_{-\infty}^{\epsilon_2} d\epsilon_1 \Lambda_1(\epsilon_1) e^{i(\omega_{10} - \omega)\epsilon_1} + \langle 0 | \vec{u} \cdot \hat{e}_1 | 1 \rangle \langle 1 | \vec{u} \cdot \hat{e}_2 | 0 \rangle \langle 0 | \vec{u} \cdot \hat{e}_3 | 1 \rangle \\ & \cdot e^{i(\vec{k}_3 + \vec{k}_2 - \vec{k}_1) \cdot \vec{r}} \int_{-\infty}^t e^{d\epsilon_3 \Lambda_3(\epsilon_3)} e^{i(\omega_{10} - \omega)\epsilon_3} \int_{-\infty}^{\epsilon_3} d\epsilon_2 \Lambda_2(\epsilon_2) e^{i(\omega_{10} - \omega)\epsilon_2} \int_{-\infty}^{\epsilon_2} d\epsilon_1 \Lambda_1^*(\epsilon_1) e^{-i(\omega_{10} - \omega)\epsilon_1} \Big| \end{aligned}$$

Table 1

XBL 8110-11708



$$(t_e)_G = \frac{1}{2} \frac{k_s}{k_s} \cdot (k_1 \epsilon_{10} + k_2 \epsilon_{20} - k_3 \epsilon_{30}) \geq \epsilon_{30} \quad \text{possible for (a), (b), (c)}$$

$$(t_e)_S = -\frac{\Delta\omega_{21}^i}{\Delta\omega_{10}^i} (\epsilon_{30} - \epsilon_{20}) + \epsilon_{10} \geq \epsilon_{30} \quad \text{possible only if } \frac{\Delta\omega_{21}^i}{\Delta\omega_{10}^i} \leq -\frac{\epsilon_{30} - \epsilon_{10}}{\epsilon_{30} - \epsilon_{20}}$$

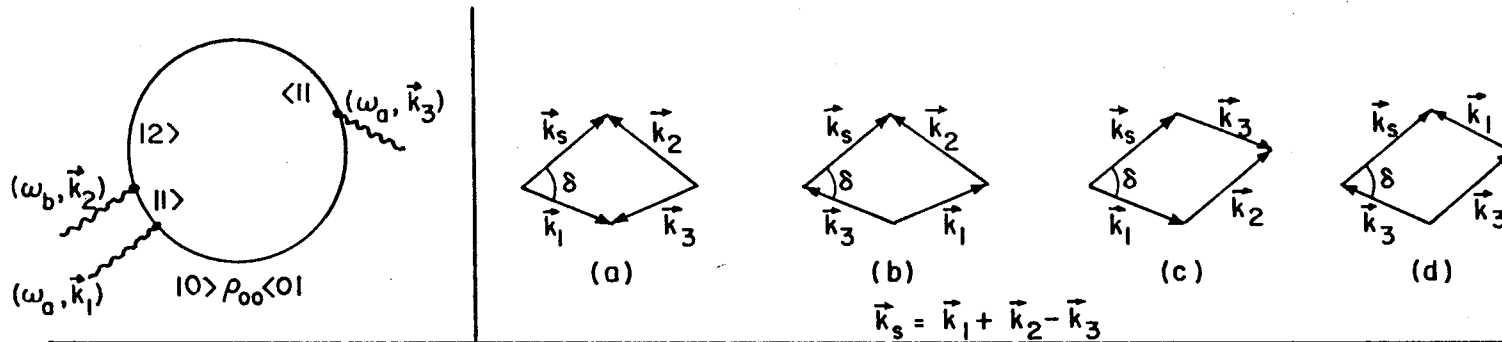
$$\rho^{(3)}(\omega_a, t_e) = -\left(\frac{1}{2i\hbar}\right)^3 e^{i(\vec{k}_s \cdot \vec{r} - \omega_{10} t_e)} \langle 1 | \vec{u} \cdot \hat{e}_3 | 2 \rangle \langle 2 | \vec{u} \cdot \hat{e}_2 | 1 \rangle \langle 1 | \vec{u} \cdot \hat{e}_1 | 0 \rangle \langle 1 | \rho_{00} \langle 0 |$$

$$e^{-i[\phi_{10}(t_e - t_{e3}) + \phi_{20}(t_{e3} - t_{e2}) + \phi_{10}(t_{e2} - t_{e1})]}$$

$$\times \int_{-\infty}^t d\tau_3 e^{-i(\omega_{21} - \omega_b)\tau_3} \Lambda_3(\tau_3) \int_{-\infty}^{\tau_3} d\tau_2 e^{i(\omega_{21} - \omega_b)\tau_2} \Lambda_2(\tau_2) \int_{-\infty}^{\tau_2} d\tau_1 e^{i(\omega_{10} - \omega_a)\tau_1} \Lambda_1(\tau_1)$$

XBL 8110-11709

Table 2(a)



$$(t_e)_G = \frac{1}{k_s} \vec{k}_s \cdot (\vec{k}_1 \epsilon_{10} + \vec{k}_2 \epsilon_{20} - \vec{k}_3 \epsilon_{30}) \geq \epsilon_{30} \quad \text{possible for (a), (b), (d)}$$

$$(t_e)_S = -\frac{\Delta\omega'_{10}}{\Delta\omega'_{21}} (\epsilon_{30} - \epsilon_{10}) + \epsilon_{20} \geq \epsilon_{30} \quad \text{possible if } \frac{\Delta\omega'_{10}}{\Delta\omega'_{21}} \leq -\frac{\epsilon_{30} - \epsilon_{20}}{\epsilon_{30} - \epsilon_{10}}$$

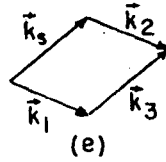
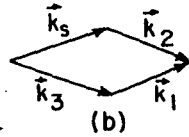
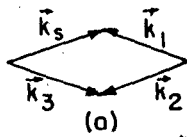
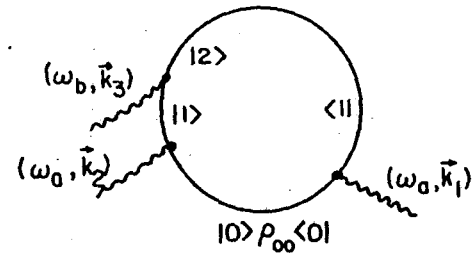
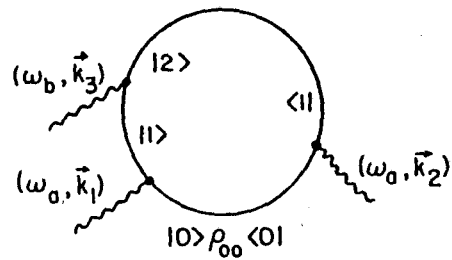
$$v^{(3)}(\omega_b, t_e) = \left(\frac{1}{2i\hbar}\right)^3 e^{i(\vec{k}_s \cdot \vec{r} - \omega_{21} t_e)} \langle 2 | \vec{v} \cdot \hat{e}_2 | 1 \rangle \langle 1 | \vec{v} \cdot \hat{e}_1 | 0 \rangle \langle 0 | \vec{v} \cdot \hat{e}_3 | 1 \rangle \langle 12 | \rho_{00} \langle 1 |$$

$$\times e^{-i[\phi_{21}(t_e - \tau_{30}) + \phi_{20}(\tau_{30} - \tau_{20}) + \phi_{10}(\tau_{20} - \tau_{10})]}$$

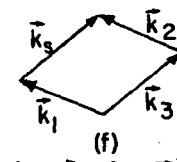
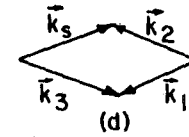
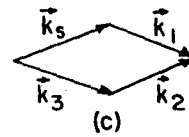
$$\times \int_{-\infty}^t d\epsilon_3 e^{-i(\omega_{10} - \omega_a)\epsilon_3} \Lambda_3^*(\epsilon_3) \int_{-\infty}^{\epsilon_3} d\epsilon_2 e^{i(\omega_{21} - \omega_b)\epsilon_2} \Lambda_2(\epsilon_2) \int_{-\infty}^{\epsilon_2} d\epsilon_1 e^{i(\omega_{10} - \omega_a)\epsilon_1} \Lambda_1(\epsilon_1)$$

XBL 8110-11710

Table 2(b)



$$\vec{k}_s = \vec{k}_3 - \vec{k}_2 + \vec{k}_1$$



$$\vec{k}_s = \vec{k}_3 + \vec{k}_2 - \vec{k}_1$$

$$(t_e)_G = \frac{1}{2} \frac{\vec{k}_s}{k_s} \cdot (\vec{k}_3 \epsilon_{30} - \vec{k}_2 \epsilon_{20} + \vec{k}_1 \epsilon_{10}) \geq \epsilon_{30} \text{ possible for all cases}$$

$$(t_e)_S = -\frac{\Delta\omega'_{10}}{\Delta\omega'_{21}} (\epsilon_{20} - \epsilon_{10}) + \epsilon_{30} \geq \epsilon_{30} \text{ possible if } \frac{\Delta\omega'_{10}}{\Delta\omega'_{21}} \leq 0$$

$$(t_e)_G = \frac{1}{2} \frac{\vec{k}_s}{k_s} \cdot (\vec{k}_3 \epsilon_{30} + \vec{k}_2 \epsilon_{20} - \vec{k}_1 \epsilon_{10}) \geq \epsilon_{30} \text{ possible for all cases}$$

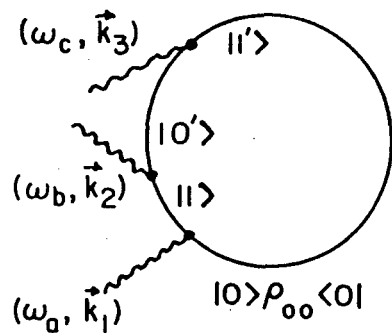
$$(t_e)_S = \frac{\Delta\omega'_{10}}{\Delta\omega'_{21}} (\epsilon_{20} - \epsilon_{10}) + \epsilon_{30} \geq \epsilon_{30} \text{ possible if } \frac{\Delta\omega'_{10}}{\Delta\omega'_{21}} \geq 0$$

$$u^{(3)}(\omega_b, t_e) = \left(\frac{1}{2i\hbar}\right)^3 e^{i(\vec{k}_s \cdot \vec{r} - \omega_a t_e)} e^{-i\phi_{21}(t_e - \epsilon_{30}) + i\phi_{11}(\epsilon_{30} - \epsilon_{20}) + i\phi_{10}(\epsilon_{20} - \epsilon_{10})} (|2\rangle_{00} \langle 1|)$$

$$\begin{aligned} & \times \langle 2|\vec{u} \cdot \hat{e}_3|1\rangle \int_{-\infty}^t e^{i(\omega_{21} - \omega_b)\epsilon_3} \Lambda_3(\epsilon_3) \left[ \langle 1|\vec{u} \cdot \hat{e}_1|0\rangle \langle 0|\vec{u} \cdot \hat{e}_2|1\rangle \int_{-\infty}^{\epsilon_3} d\epsilon_2 e^{-i(\omega_{10} - \omega_a)\epsilon_2} \Lambda_2^*(\epsilon_2) \right. \\ & \left. \times \int_{-\infty}^{\epsilon_2} d\epsilon_1 e^{i(\omega_{10} - \omega_a)\epsilon_1} \Lambda_1(\epsilon_1) + \text{Complex Conjugate} \right] \end{aligned}$$

XBL 8110-11711

Table 2(c)



$$\omega = \omega_c - \omega_b + \omega_a$$

$$\vec{k}_s = \vec{k}_3 - \vec{k}_2 + \vec{k}_1$$

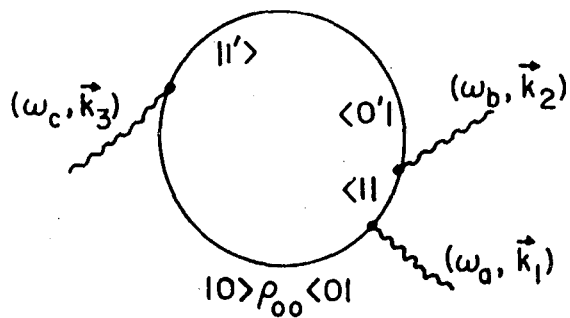
$$(t_e)_G = \frac{1}{2} \frac{\vec{k}_s}{k_s} \cdot (\vec{k}_3 \epsilon_{30} - \vec{k}_2 \epsilon_{20} + \vec{k}_1 \epsilon_{10})$$

$$(t_e)_S = \frac{1}{\Delta\omega_{1'0}^i} (\Delta\omega_{1'0}^i \epsilon_{30} - \Delta\omega_{10}^i \epsilon_{20} + \Delta\omega_{10}^i \epsilon_{10})$$

$$\begin{aligned} \rho^{(3)}(\omega, t_e) = & - \left( \frac{1}{2i\hbar} \right)^3 e^{i(\vec{k}_s \cdot \vec{r} - \omega_{1'0} t_e)} \langle 1' | \vec{\mu} \cdot \hat{e}_3 | 0' \rangle \langle 0' | \vec{\mu} \cdot \hat{e}_2 | 1 \rangle \langle 1 | \vec{\mu} \cdot \hat{e}_1 | 0 \rangle \langle 1' | \rho_{00} \langle 0 | \\ & \times e^{-[\phi_{1'0}(t_e - \epsilon_{30}) + \phi_{0'0}(\epsilon_{30} - \epsilon_{20}) + \phi_{10}(\epsilon_{20} - \epsilon_{10})]} \\ & \times \int_{-\infty}^t e^{i(\omega_{1'0} - \omega_c) \epsilon_3} d\epsilon_3 \Lambda_3(\epsilon_3) \int_{-\infty}^{\epsilon_3} e^{-i(\omega_{10} - \omega_b) \epsilon_2} d\epsilon_2 \Lambda_2^*(\epsilon_2) \int_{-\infty}^{\epsilon_2} e^{i(\omega_{10} - \omega_a) \epsilon_1} d\epsilon_1 \Lambda_1(\epsilon_1) \end{aligned}$$

XBL 8110-11712

Table 3



$$\omega = \omega_c + \omega_b - \omega_a$$

$$\vec{k}_s = \vec{k}_3(\omega_c) + \vec{k}_2(\omega_b) - \vec{k}_1(\omega_a)$$

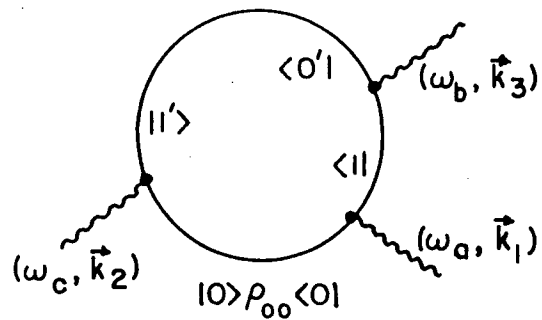
$$(t_e)_G = \frac{1}{k_s} \vec{k}_s \cdot (\vec{k}_3 \xi_{30} + \vec{k}_2 \xi_{20} - \vec{k}_1 \xi_{10})$$

$$(t_e)_S = \frac{1}{\Delta\omega_{1'0'}} (\Delta\omega_{1'0'} \xi_{30} + \Delta\omega_{10'} \xi_{20} - \Delta\omega_{10'} \xi_{10})$$

$$\begin{aligned} \rho^{(3)}(\omega, t_e) = & - \left( \frac{1}{2i\hbar} \right)^3 e^{i(\vec{k}_s \cdot \vec{r} - \omega_{1'0'} t_e)} \langle 1' | \vec{\mu} \cdot \hat{e}_3 | 0 \rangle \langle 0 | \vec{\mu} \cdot \hat{e}_1 | 1 \rangle \langle 1 | \vec{\mu} \cdot \hat{e}_2 | 0 \rangle \langle 1' | \rho_{00} \langle 0' | \\ & \times e^{-[\phi_{1'0'}(t_e - \xi_{30}) + \phi_{0'0'}(\xi_{30} - \xi_{20}) + \phi_{10'}(\xi_{20} - \xi_{10})]} \\ & \times \int_{-\infty}^{t_e} d\xi_3 e^{i(\omega_{1'0'} - \omega_c)\xi_3} \Lambda_3(\xi_3) \int_{-\infty}^{\xi_3} d\xi_2 e^{i(\omega_{10'} - \omega_b)\xi_2} \Lambda_2(\xi_2) \int_{-\infty}^{\xi_2} d\xi_1 e^{-i(\omega_{10'} - \omega_a)\xi_1} \Lambda_1^*(\xi_1) \end{aligned}$$

XBL 8110-11713

Table 4(a)



$$\omega = \omega_c + \omega_b - \omega_a$$

$$\vec{k}_s = \vec{k}_3(\omega_b) + \vec{k}_2(\omega_c) - \vec{k}_1(\omega_a)$$

$$(t_e)_G = \frac{1}{k_s^2} \vec{k}_s \cdot (\vec{k}_3 \epsilon_{30} + \vec{k}_2 \epsilon_{20} - \vec{k}_1 \epsilon_{10})$$

$$(t_e)_S = \frac{1}{\Delta\omega_{1'0'}} (\Delta\omega_{10'}^1 \epsilon_{30} + \Delta\omega_{1'0'}^1 \epsilon_{20} - \Delta\omega_{10'}^1 \epsilon_{10})$$

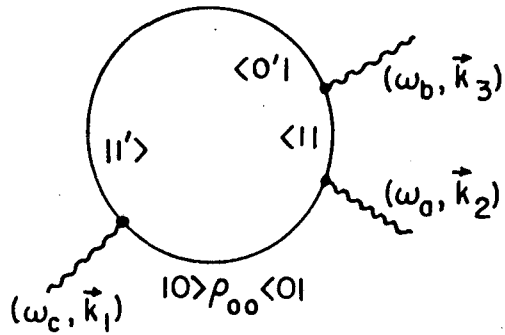
$$\mu^{(3)}(\omega, t_e) = - \left( \frac{1}{2i\hbar} \right)^3 e^{i(\vec{k}_s \cdot \vec{r} - \omega_{1'0'} t_e)} \langle 1' | \vec{v} \cdot \hat{e}_2 | 0 \rangle \langle 0 | \vec{v} \cdot \hat{e}_1 | 1 \rangle \langle 1 | \vec{v} \cdot \hat{e}_2 | 0' \rangle (|1'\rangle_{00} \langle 0'|)$$

$$\times e^{-[\phi_{1'0'}(t_e - \xi_{30}) + \phi_{1'1}(\xi_{30} - \xi_{20}) + \phi_{10}(\xi_{20} - \xi_{10})]}$$

$$\times \int_{-\infty}^t d\xi_3 e^{i(\omega_{10'} - \omega_b)\xi_3} \Lambda_3(\xi_3) \int_{-\infty}^{\xi_3} d\xi_2 e^{i(\omega_{1'0'} - \omega_c)\xi_2} \Lambda_2(\xi_2) \int_{-\infty}^{\xi_2} d\xi_1 e^{-i(\omega_{10'} - \omega_a)\xi_1} \Lambda_1^*(\xi_1)$$

XBL 8110-11714

Table 4(b)



$$\omega = \omega_c + \omega_b - \omega_a$$

$$\vec{k}_s = \vec{k}_s(\omega_b) - \vec{k}_2(\omega_a) + \vec{k}_1(\omega_c)$$

$$(t_e)_G = \frac{1}{k_s} \vec{k}_s \cdot (\vec{k}_3 \xi_{30} - \vec{k}_2 \xi_{20} + \vec{k}_1 \xi_{10})$$

$$(t_e)_S = \frac{1}{\Delta\omega_{1'0}} (\Delta\omega_{1'0} \xi_{30} - \Delta\omega_{1'0} \xi_{20} + \Delta\omega_{1'0} \xi_{10})$$

$$\rho^{(3)}(\omega, t_e) = - \left( \frac{1}{2i\hbar} \right)^3 e^{i(\vec{k}_s \cdot \vec{r} - \omega t_e)} \langle 1' | \vec{\mu} \cdot \hat{e}_1 | 0 \rangle \langle 0 | \vec{\mu} \cdot \hat{e}_2 | 1 \rangle \langle 1 | \vec{\mu} \cdot \hat{e}_3 | 0' \rangle \langle 1' | \rho_{00} | 0' \rangle$$

$$\times e^{-[\phi_{1'0}(t_e - \xi_{30}) + \phi_{1'1}(\xi_{30} - \xi_{20}) + \phi_{1'0}(\xi_{20} - \xi_{10})]}$$

$$\times \int_{-\infty}^{t_e} d\xi_3 e^{i(\omega_{10} - \omega_b)\xi_3} \Lambda_3(\xi_3) \int_{-\infty}^{\xi_3} d\xi_2 e^{-i(\omega_{10} - \omega_a)\xi_2} \Lambda_2(\xi_2) \int_{-\infty}^{\xi_2} d\xi_1 e^{i(\omega_{1'0} - \omega_c)\xi_1} \Lambda_1^*(\xi_1)$$

XBL 8110-11715

Table 4(c)

This report was done with support from the Department of Energy. Any conclusions or opinions expressed in this report represent solely those of the author(s) and not necessarily those of The Regents of the University of California, the Lawrence Berkeley Laboratory or the Department of Energy.

Reference to a company or product name does not imply approval or recommendation of the product by the University of California or the U.S. Department of Energy to the exclusion of others that may be suitable.

TECHNICAL INFORMATION DEPARTMENT  
LAWRENCE BERKELEY LABORATORY  
UNIVERSITY OF CALIFORNIA  
BERKELEY, CALIFORNIA 94720